UNIVERSITÀ
DI PAVIA

DIPARTIMENTO DI SCIENZE DEL FARMACO

Direttore Chiar.ma Prof.ssa Simona Collina

LAUREA MAGISTRALE A CICLO UNICO IN FARMACIA

Genomic and functional study of Cornelia de Lange syndrome in iPSC-derived cellular models

Relatore: Marco Racchi

Correlatori: Mineko Terao
Enrico Garattini

Tesi di Laurea Magistrale a Ciclo Unico di
Eva Mercurio

Anno Accademico 2025/2026

TABLE OF CONTENTS

LIST OF ABBREVIATIONS

ALL Acute lymphoblastic leukemia
AML Acute myeloid leukemia
ASXL1 Additional Sex Combs Like 1
BSA Bovine Serum Albumin
BMP4 Bone Morphogenetic Protein 4
CdLS Cornelia de Lange syndrome
DMSO Dimethy sulfoxide
DNA Deoxyribonucleic acid
DNMT3B DNA methyltransferase 3B
DPBS Dulbecco's Modified Eagle Medium
DPP6 Dipeptidyl peptidase-like protein 6
ECG Electrocardiogram
EDTA Ethylenediaminetetraacetic acid
ESC Embryonic stem cell
FACS Fluorescence-Activated Cell Sorting
FBS Fetal bovine serum
FGF2 Fibroblast growth factor 2
FLT3 FLT3 Ligand
FOXA2 Forkhead box A2
FOXP2 Forkhead box P2
GERD Gastroesophageal reflux disease
GM-CSF Granulocyte-Macrophage colony-stimulating factor
HDAC8 Histone deacetylase 8
HEAT Huntingtin, elongation factor 3, protein phosphatase 2A
hiPSC Human induced pluripotent stem cells
HHEX Hematopoietically expressed homeobox
HPC Hematopoietic progenitor cells
iPSC Induced pluripotent stem cell
KLF4 Kruppel-like factor 4
M0 Non-polarized macrophages
M1 Classically activated pro-inflammatory macrophages
M2 Alternatively activated anti-inflammatory macrophages
MAU2 MAU2 cohesin loading factor
M-CSF Macrophage colony-stimulating factor
MDS Myelodysplastic syndromes
MPC Myeloid progenitor cells
MYC Avian Myelocytomatosis viral oncogene
NANOG Nanog homeobox
NIPBL Nipped-B-like protein
OCT3/4 Octamer-binding transcription factor 3/4
OCT4 Octamer-binding transcription factor 4

PAX6 Paired box 6
PBMC Peripheral blood mononuclear cells
PBS Phosphate Buffered Saline
PCR Polymerase chain reaction
PDS5 PDS5 cohesin-associated factor A
POU5F1 POU class 5 homeobox 1
PROX1 Prospero homeobox 1
qPCR Quantitative Polymerase Chain Reaction
qRT-PCR Quantitative Reverse Transcription PCR
RAD21 RAD21 cohesin complex component
RNA-seq RNA sequencing
ROCK Rho-associated protein kinase
RUNX1 Runt-related Transcription Factor 1
SCF Stem Cell Factor
SMC1A Structural maintenance of chromosomes protein 1A
SMC3 Structural maintenance of chromosomes protein 3
SNAL2 SNAI2 (Snail family transcriptional repressor 2)
SOX2 SRY-box transcription factor 2
SOX17 SRY-box transcription factor 17
STAG2 Stromal Antigen 2
TAD Topologically associating domain
TPO Thrombopoietin
TRA-1-60 Tumor rejection antigen 1-60
VEGF Vascular Endothelial Growth Factor
WAPL WAPL cohesin release factor
WGS Whole genome sequencing
ZNF Zinc finger protein

CHAPTER 1- ABSTRACT

Cornelia de Lange Syndrome (CdLS) is a multisystem genetic disorder characterized by craniofacial abnormalities, limb malformations, growth retardation, intellectual disability, and developmental delay. This syndrome belongs to the group of cohesinopathies, as it is caused by mutations in genes encoding components of the cohesin complex, which plays a crucial role in regulating gene expression and chromatin organization. Due to the associated disruption of chromatin structure, CdLS is also classified among chromatinopathies.

Alterations in chromatin organization have recently been recognized as key contributors to the pathogenesis of myeloid neoplasms, a group of clonal disorders of hematopoietic stem cells caused by mutations in genes involved in transcriptional regulation, epigenetic control, and RNA splicing. In particular, mutations affecting components of the cohesin complex (such as STAG2, RAD21, SMC1A, SMC3, and PDS5B) and its regulatory proteins (including NIPBL, MAU2, and HDAC8) play a critical role in hematopoietic stem cell function. These mutations are found in approximately 20% of patients with acute myeloid leukemia (AML), often in association with mutations in other genes such as *NPM1* (Nucleophosmin), *FLT3* (FMS-like tyrosine kinase), *RUNX1* (Runt-related transcription factor 1), and *ASXL1* (Additonal sex-combs-like).

In light of the link between cohesin dysfunction, chromatin disorganization, and leukemogenesis, the present study aims to establish an *in vitro* differentiation system of induced pluripotent stem cells (iPSCs) along the myeloid hematopoietic lineage using this model of chromatinopathy. To this end, iPSC lines derived from CdLS patients was used alongside control iPSC lines obtained from healthy individuals. These cell lines were generated and available at the Laboratory of Molecular Biology of the Mario Negri Institute for Pharmacological Research.

The objective of this work is to establish an in vitro differentiation system based on iPSC to understand the pathogenic mechanisms underlying CdLS. In particular, the final goal of the project is focused on the role of cohesin and chromatin alterations in leukemic transformation.

CHAPTER 2 – INTRODUCTION

2.1. Cornelia De Lange Syndrome

Cornelia de Lange Syndrome (CdLS) is a rare genetic disorder primarily affecting the pediatric population. It is classified as a cohesinopathy and is mainly characterized by growth and developmental delays. The syndrome was first described in 1933 by Dr. Cornelia de Lange, a Dutch pediatrician who identified two children exhibiting the characteristic phenotypic features of the disorder. The estimated prevalence varies from 0.5 to 10 cases per 100,000 individuals; however, due to intermediate phenotypes and diagnostically challenging cases, the true incidence is likely underestimated (Boyle *et al.*, 2015; Selicorni *et al.*, 2021). In the majority of patients (>65%), mutations in the *NIPBL* gene have been identified, with an estimated prevalence of approximately 1 in 30,000 live births. However, due to the marked phenotypic heterogeneity of the syndrome, it is believed that a significant proportion of affected individuals remain undiagnosed (Boyle *et al.*, 2015). In the case under investigation in this thesis, CdLS is associated with a missense point mutation**.** The genetic alteration corresponds to a G5483A nucleotide substitution**,** which results in the production of a protein carrying the Arg1828Gln variant. This mutation, in line with other point variants previously described in the *NIPBL* gene, is considered to have a causal role in the onset of the disorder. Current evidence regarding the precise molecular functions of NIPBL protein and its interaction with the cohesin complex remains limited, and continues to be the subject of active research.

CdLS is characterized by a wide range of clinical manifestations affecting multiple organ system. Among the most characteristic features are pre- and postnatal growth retardation, intellectual disability of variable severity, and distinctive craniofacial dysmorphisms. This includes microcephaly, synophrys (arched eyebrows that meet at the midline), long eyelashes, a short nose with depressed or triangular nasal tip and a long smooth philtrum. At the somatic level, patients exhibit short stature due to persistent growth retardation and upper limb malformations that impair functionality, including radio-ulnar synostosis and limited elbow flexion-extension caused by proximal radial head hypoplasia. Patients often present with thin lips with downturned corners, micrognathia, short neck, and small chin**,** as well as oral anomalies such as a high-arched palate and dental malformations (Kline, Barr e Jackson, 1993). Hirsutism is commonly observed, particularly on the forearms and lumbosacral region. In a subset of cases, cutis marmorata, a vascular anomaly characterized by

bluish-purple marbled skin patches, can be observed (Ascaso *et al.*, 2024). Lower limb involvement is rare, although scoliosis may occur.

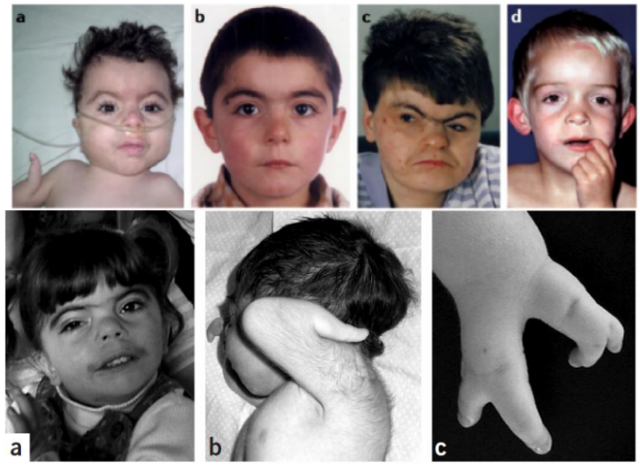

Figure 1. Facial phenotype of individuals with Cornelia de Lange syndrome (fonte: "Kline et al, 1993")

Psychomotor and cognitive impairments range from mild to severe depending on the overall severity of the syndrome. The language domain is particularly affected: only 10–15% of patients exhibit minimal or no difficulties in verbal communication, while the remaining 85–90% experience significant deficits, with approximately 30% unable to communicate verbally. Behavioral problems are also common, including hyperactivity, attention deficits, aggressiveness, shyness, obsessive-compulsive behaviors, and sleep disturbances (Ajmone *et al.*, 2014), often linked to frustration arising from impaired communication abilities. Gastrointestinal involvement is significant, with over 90% of patients presenting gastroesophageal reflux disease (GERD), which can cause vomiting, nighttime agitation, and hyperactivity. GERD often persists long-term and may lead to complications such as aspiration pneumonia and feeding difficulties, especially in neonates and children under five years old, further aggravated by cleft palate, micrognathia, and reduced oral mucosa tone (Luzzani *et al.*, 2003).

Cardiovascular anomalies occur in approximately 25–30% of patients, including congenital heart defects (CHD) such as ventricular and atrial septal defects and hypoplastic left heart syndrome (Chatfield *et al.*, 2012). Disease severity and mutation type influence the incidence and severity of CHD, with mutations in *NIPBL, SMC1A*, and *SMC3* being associated with cardiac defects. Routine ECG screening in children with CdLS is essential for early detection and management of potential complications. Neurological and sensory manifestations frequently include hearing loss and recurrent otitis (often due to narrow or stenotic auditory canals), sinusitis, myopia, ptosis, and blepharitis (Marchisio *et al.*, 2014).

Peripheral neuropathies, affecting approximately 20–25% of patients, can result in reduced pain sensitivity (Kline *et al.*, 2007).

The leading cause of mortality in CdLS is gastrointestinal complications**,** alongside diaphragmatic hernia, secondary pneumonia, and intestinal volvulus**,** which may occur early in life and reduce life expectancy (Kline *et al.*, 2007; Piché *et al.*, 2019). In a cohort study of 426 individuals conducted by Dr. Samantha Schrier at the Children's Hospital of Philadelphia, survival rates varied with life stages: 12 years and 9 months for patients surviving the neonatal period, 16 years and 2 months for those surviving the first year of life, and 28 years and 2 months for individuals reaching adulthood. Respiratory causes predominate in neonates, while gastrointestinal complications become more frequent with age. Non-specific early symptoms, such as vomiting, can delay diagnosis and contribute to increased morbidity and mortality.

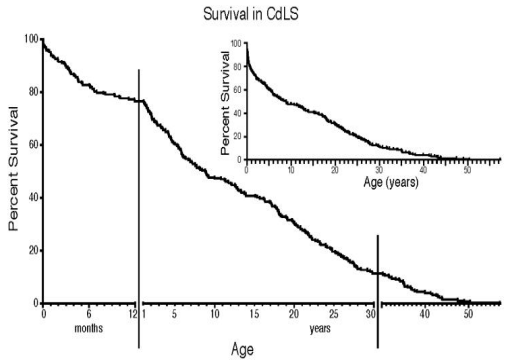

Figure 2. Survival curve of the cohort analyzed in the study by Schrier et al., 2011, illustrating the prognosis of the disease.

2.1.1 Cornelia de Lange Syndrome: diagnosis

The diagnosis of Cornelia de Lange syndrome (CdLS) should be considered as a clinical spectrum characterized by a wide variability in phenotypic expression which depends on the type and severity of mutations affecting genes encoding subunits or regulators of the cohesin complex. It is important to emphasize that CdLS belongs to the group of cohesinopathies, although not all alterations involving the cohesin complex necessarily lead to this specific syndromic presentation (Kline *et al.*, 2007). From a clinical perspective, the diagnosis can be suspected as early as the neonatal period, based on the recognition of phenotypic and behavioral features typical of the syndrome like distinctive craniofacial dysmorphisms, growth retardation, limb abnormalities, and neurodevelopmental delay. However, in cases with milder or atypical

forms, diagnosis may be challenging and may require several years, particularly in patients with attenuated phenotypes whose symptomatology may overlap with that of autism spectrum disorders. It has been reported that the majority of diagnoses are made by eight years of life. Beyond this age, clinical recognition becomes more difficult, increasing the risk of underestimation of the true incidence.

Prenatal diagnosis may be considered in families with a positive history of CdLS. Obstetric ultrasound between the 18th and 20th weeks of gestation con reveal fetal anatomy and the identification of structural anomalies typical of the syndrome (e.g., intrauterine growth restriction, limb defects, craniofacial anomalies, congenital heart defects). However, ultrasound alone is not a definitive diagnostic tool, but rather a useful aid to guide further investigations by gynecologists, radiologists, and obstetricians. A definitive prenatal diagnosis is possible only through targeted genetic testing, particularly in the presence of a mutation already identified in an affected family member.

Postnatal confirmation of CdLS is based on molecular analyses which allow the identification of mutations in genes involved in the cohesin complex like *NIPBL, SMC1A, SMC3, RAD21, HDAC8, BRD4*, and others. These methods enable confirmation of the clinical suspicion in approximately 80% of cases. However, several limitations including the high costs of genetic testing which reduce accessibility, particularly in low-income countries or in healthcare systems lacking adequate insurance coverage and the presence of somatic mosaicism in approximately 20% of patients. Mutation may not be detectable in peripheral blood samples and may require analysis of other tissues, such as skin fibroblasts or buccal epithelial cells.

In conclusion, the diagnosis of CdLS is based on an integrated approach that combines clinical criteria, prenatal investigations, and molecular confirmation, supported by a multidisciplinary team of specialists like geneticists, pediatricians, neurologists, cardiologists, radiologists, and psychologists, in order to ensure a comprehensive and timely evaluation of the patient.

2.1.2 Cornelia de Lange: therapy

The management of Cornelia de Lange syndrome requires an early and multidisciplinary approach, due to the complexity and multisystem nature of the disorder. From early childhood, it is necessary to rely on a team composed of specialists from different disciplines, including otolaryngologists, cardiologists, gastroenterologists, endocrinologists, urologists, dentists, and pediatric neuro-rehabilitation therapists

(Mikołajewska, 2013). Continuous interaction between these professionals allows the various manifestations of the disorder to be addressed in an integrated and patient-specific manner, with interventions tailored to the severity of each individual case. Among therapeutic options, speech therapy plays a central role and is often combined with exercises aimed at strengthening the musculature involved in vocalization. These interventions are often combined with exercises aimed to improve communication skills and reduce the relational difficulties arising from language deficits (Grados, Alvi e Srivastava, 2017).

Pharmacological therapy is used to manage concomitant conditions such as epilepsy, conjunctivitis, and cardiac diseases, while in more severe cases it may also be employed to address depression and stress, although conservative strategies (non-pharmacological approaches) are preferred whenever possible. Surgical intervention becomes necessary when complications such as gastroesophageal reflux, dental anomalies, or limb malformations are present. In patients with hearing impairment, the use of hearing aids represents an important measure for improving quality of life and promoting social participation. In parallel, constant neuromotor rehabilitation is essential to support motor development and promote functional autonomy (Mikołajewska, 2013).

An experimental intervention worthy of mention is the CLOSER study in Italy which investigates the efficacy of lithium carbonate for its potential activation of the WNT pathway in the treatment of CdLS. Finally, psychological support for families represents a crucial aspect of patient management. The daily care of individuals affected by a rare and complex condition such as Cornelia de Lange syndrome can generate high levels of stress and negatively impact the mental health of caregivers. Providing adequate psychological support contributes not only to overall family well-being, but also the effectiveness of therapeutic interventions.

2.1.3 Cornelia de Lange Syndrome: genetic causes

Cornelia de Lange syndrome (CdLS) belongs to the group of cohesinopathies, a class of genetic disorders caused by mutations in genes encoding components of the cohesin complex or its regulators. Among these conditions, CdLS represents the most extensively studied form. The genes most frequently associated with CdLS include *NIPBL, SMC1A, SMC3, RAD21,* and *HDAC8*, all of which encode components of the cohesin complex or its regulators. The cohesion complex is composed of four core subunits: *SMC1* (Structural Maintenance of Chromosomes 1), *SMC3, RAD21* (also known as SCC1), and *SCC3* (SA1/2). These components interact with several accessory factors such as NIPBL, MAU2, HDAC8, WAPL, PDS5, ESCO1/2, and PLK1, which regulate cohesin loading, stability, and function. (Piché *et al.*, 2019).

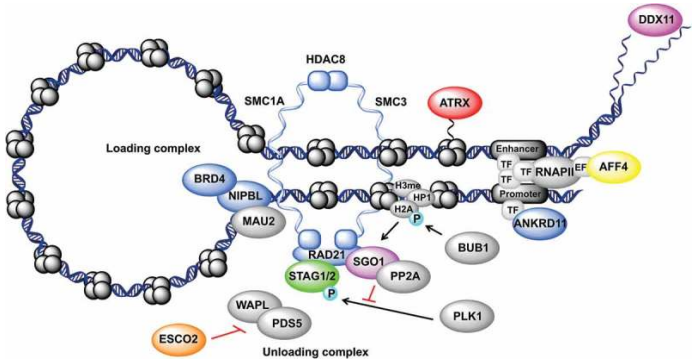

Figure 3. ***Components*** *(SMC1, SMC3, RAD21, and STAG1/2)* ***and partners of the cohesin complex.*** *Colors indicate proteins whose mutated forms are involved in cohesinopathies. Blue: CdLS (NIPBL, HDAC8, SMC1A, SMC3, RAD21, BRD4, ANKRD11), Orange: RBS (Pichè et al, 2019)*

Structurally, cohesion forms a ring-like complex capable of encircling DNA. This configuration enables its fundamental biological functions, which can be divided into canonical and non-canonical roles. Canonical functions include sister chromatid cohesion, regulation of replication fork progression, correct kinetochore orientation, maintenance of chromatin architecture. Non-canonical functions include regulation of transcription, DNA repair through homologous recombination, formation of Topologically Associated Domains (TADs).

The foundations of this discovery date back to studies by Koshland and Nasmyth, who in the yeast *Saccharomyces cerevisiae* identified the genes *SMC1, SMC3, RAD21,* and *SCC3* as essential for chromatid cohesion during the S phase of the cell cycle (Nasmyth e Haering, 2009). At the molecular level, SMC1 and SMC3 proteins belong to the SMC family and share a primary organization characterized by an ATPase head domain, derived from the interaction of the N- and C-terminal ends, a hinge region that mediates dimerization and long coiled-coil domains that

connect the head and hinge, forming the characteristic “V”-shaped structure (Melby et al., 1998).

RAD21 is positioned between the two heads, linking SMC3 at the N-terminus and SMC1 at the C-terminus, closing the ring. Its central region interacts with regulatory proteins such as SA1/2 , PDS5, and NIPBL, contributing to the dynamic regulation of the complex. (*Closing the cohesin ring: Structure and function of its Smc3-kleisin interface*, sine data). Cohesin loading onto chromatin occurs primarily during the G1 phase through the *NIPBL–MAU2* complex, while cohesion stabilization is ensured by acetylation of *SMC3* by *ESCO1/2*, which prevents *WAPL/PDS5*-mediated cohesin removal during S and G2. Chromatid separation during mitosis requires proteolysis of *RAD21* by separase, allowing recycling of the subunits (Nasmyth e Haering, 2009). Beyond chromosome segregation, cohesin is also crucial for the regulation of gene transcription.
Studies in *Drosophila* have demonstrated that the complex can modulate gene expression independently of chromatid cohesion (Heidinger-Pauli *et al.*, 2010), strengthening its association with chromatin. For example, cohesin is enriched at genes encoding rRNA, which are essential for ribosome biogenesis (Laloraya, Guacci e Koshland, 2000). Through the formation of chromatin loops, cohesin contributes to the spatial organization to the genome and regulates promoter-enhancer interactions. The presence of the architectural CTCF (CCCTC-binding factor) is crucial in this process: in its absence, transcription-inhibitory loops prevail, whereas in its presence, structures favoring gene activation are formed.

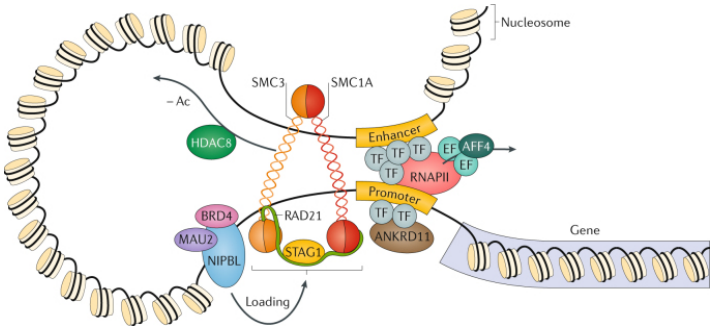

Figure 4. Chormatin loops in absence of CTCF (Kline et al, 2019)

The structure and functions of cohesin are highly evolutionarily conserved, with minimal amino acid differences (<0.5%) between species (White e Erickson, 2009). In humans, approximately 84% of patients with CdLS carry mutations in cohesin genes or their regulators, with a predominance of *NIPBL* (~60%) (Kline *et al.*, 2018). These mutations are

generally autosomal dominant and arise as *de novo* events, although germline mosaicism represents a significant transmission risk (>50%). In cases of somatic mosaicism, the mutation may not be detectable in peripheral blood, making the analysis of other tissues, such as buccal mucosa cells or skin fibroblasts. (Huisman *et al.*, 2013). Mutations in *SMC1A* and *SMC3* (approximately 5% of cases) are generally associated with milder phenotypes that differ slightly from classical CdLS, such as thicker and flatter eyebrows and a broader nasal bridge 6/19/*26 10*:16:00 AM. Missense mutations in *SMC1A*, which reduce but do not abolish protein function, are compatible with survival and cause CdLS; conversely, mutations leading to complete knock-out are associated with more severe phenotypes, including seizures and severe intellectual disability (Deardorff, Noon e Krantz, 1993). Mutations in *RAD21* are also associated with milder phenotypes (Deardorff *et al.*, 2012), whereas mutations in *HDAC8*, an X-linked gene, may produce classical CdLS features but with peculiarities such as delayed closure of the cranial fontanelle. In females, random X-chromosome inactivation contributes to variability in phenotype severity, whereas this mechanism does not apply to *SMC1A*, which escapes X inactivation (Deardorff *et al.*, 2012; Decroos *et al.*, 2014). Rarer cases involve genes such as *BRD4, TAF1, TAF6,* and *AFF4*, although the number of reported cases remains limited, making genotype-phenotypes correlations less clearly defined (Moss *et al.*, 2017; Olley *et al.*, 2018). Genotype–phenotype correlation, while it is useful for diagnosis and clinical management, remains incomplete and is sometimes discordant with observed severity.

In recent years, increasing attention has been directed toward the role of NIPBL alterations in neoplastic transformation, particularly in hematological malignancies. Recent studies have shown that, in patients affected by acute myeloid leukemia (AML), mutations in the *NPM1* gene are frequently associated with a significant reduction in NIPBL expression, suggesting a functional interplay between these factors in the regulation of hematopoiesis. (Mazzola *et al.*, 2019).
Experimental models have demonstrated that NIPBL downregulation leads to an expansion of myeloid progenitors and an impairment of their differentiation, resulting in the accumulation of immature cells, a hallmark of leukemic transformation (Mazzola *et al.*, 2019). This effect is at least partially mediated by the hyperactivation of the Wnt/β-catenin signaling pathway, which plays a key role in controlling the proliferation and fate of hematopoietic stem cells.
Overall, these findings indicate that *NIPBL*, beyond its established role in embryonic development and chromatin organization, also contributes to the maintenance of hematopoietic homeostasis. Its alteration may therefore promote leukemogenesis through mechanisms involving

transcriptional dysregulation and impaired cellular differentiation, particularly in the presence of other oncogenic mutations.

In this framework, the role of chromatin disorganization and the cohesin complex in the pathogenesis of myeloid neoplasms become particularly relevant.

2.2 NIPBL and its involvement in Cornelia de Lange Syndrome

NIPBL (Nipped-B-Like protein) is a large protein composed of more than 2500 amino acid, whose structure is characterized by a distinct functional domain. The N-terminal portion is characterized by intrinsically disordered sequences, while the C-terminal portion contains numerous HEAT repeats which consist of tandems of two α-helices connected by a flexible loop. The repeats adopt a hook-like conformation and that is essential for mediating with protein-protein interaction.
NIPBL forms a stable complex with MAU2, a partner protein with a folded helical structure that plays a crucial role in stabilizing NIPBL and facilitating its localization to chromosomal regions. (Alonso-Gil e Losada, 2023).
The NIPBL-MAU2 complex acts as the main cohesin loading factor on chromatin. At the functional al level, this complex regulates several key steps in cohesin dynamics. First, it activates the ATPase activity of the SMC proteins (SMC1 and SMC3), which is essential for the function of the complex (Davidson e Peters, 2021). It mediates the trapping of DNA between the heads of SMC1 and SMC3, forming a channel. In addiction it promotes the topological entrapment of DNA within the cohesin ring and counteracts premature release mediated by the PDS5-WAPL complex.

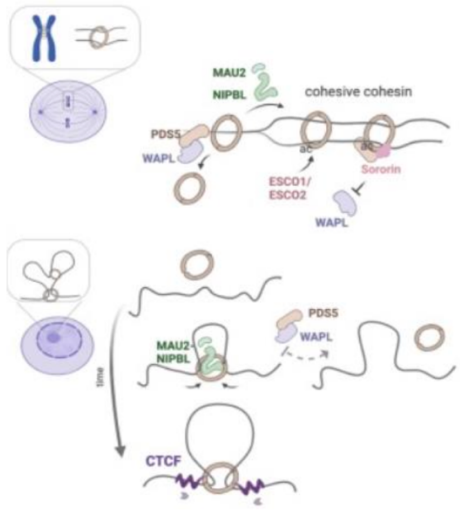

Figure 5. During sister chromatid cohesion, the cohesin complex bound to unreplicated chromatin is removed through the action of PDS5-WAPL. Subsequently, assisted by NIPBL-MAU2, a new complex binds to the sister chromatids generated from the replication fork during the S phase of the cell cycle. To prevent relase mediated by WAPL, acetylation od SMC3 occurs through the action of the acetyltransderases ESCO1/1, and Sororin is also recuited through PDS5. Thorugh the binding of the complex, the characteristic loops that allow genome folding are formed. Loop formation is enabled by interaction with CTCF, and loop relase then occurs through the action of the PDS5-WAPL complex (Alonso et al, 2023).

Beyond its role in cohesion loading, *NIPBL* is involved in multiple cellular processes. It interacts with chromatin remodelers to facilitate the formation of nucleosome-free region and associates with the MCM complex (replicative helicase) during the DNA replication, promoting early recruitment of cohesion at replication fork. Furthermore, NIPBL interacts with transcription factors and RNA polymerase II, facilitating ring extrusion and replication.

The configuration of the NIPBL-MAU2 complex in its soluble form, that is, before DNA binding, has not yet been clarified. Approximately 60% of patients affected by Cornelia de Lange syndrome (CdLS) carry mutations in *NIPBL* gene(Rollins *et al.*, 2004). These mutations are distributed throughout most of the gene, with the exception of exons 13 and 16. Different types of mutations are associated with distinct clinical phenotypes. Missense mutations are generally linked to intermediate phenotype, often without major limb anomalies and with relatively preserved cognitive development. In contrast, frameshift mutations and large deletions are typically associated with more severe forms of the syndrome. Particularly relevant are mutations affecting the HEAT repeat domains. For instance, deletion of exon 32 (H3 repeat of the HEAT domain), prevents the interaction of NIPBL with protein partners, causing severe phenotypes. Conversely, deletions involving exons 35–47 may result in milder clinical manifestations, as the truncated protein retains partial functionality (Mannini *et al.*, 2013).

NIPBL is a highly dose-dependent gene. In *Drosophila* model organisms, a 30% reduction in *Nipped-B* expression leads to cause severe transcriptional alterations and organ defects; a reduction greater than 50% leads to lethal outcomes (Rollins *et al.*, 2004). In mice, the homology with human NIPBL is 88%, and haploinsufficiency results in phenotypes comparable to those observed in CdLS patients.

In CdLS patient-derived cell lines, *NIPBL* mutations lead to a residual expression of approximately 70%, which is sufficient to induce widespread transcriptional deregulation and differentiation defects. The HEAT repeats regions, particularly H2–H4, are crucial for NIPBL function: mutations in this domain impair the interaction of NIPBL with

chromatin and regulatory proteins, leading to altered gene expression. In addition, NIPBL has been shown to interact with histone deacetylases (such as HDAC1 and HDAC3), leading to epigenetic deregulation and abnormal histone modifications (Jahnke *et al.*, 2008).

Interestingly, although *NIPBL* mutations lead to transcriptional alterations, they do not appear to directly impair the cohesive function of the cohesin complex. Experiments in murine cortical neurons have demonstrated that removal of cohesin (through RAD21 cleavage) induces transcriptional alterations and changes in the three-dimensional organization of the genome, which are reversible upon restoration of cohesion (Rollins, Morcillo e Dorsett, 1999).

In addition to its role in development, mutations and reduced expression of NIPBL have been linked to hematological malignancies. Heterozygous frameshift mutations have been identified in pediatric cases of B-cell precursor acute lymphoblastic leukemia (ALL) (Fazio *et al.*, 2017). Moreover, reduced NIPBL has been associated with progression toward AML in the presence of concomitant mutations in NPM1 (Mazzola *et al.*, 2020). Large-scale genomic studies involving more than 1600 AML patients have shown that even a single mutation in a cohesion-related gene may be sufficient for disease onset (Eckardt *et al.*, 2023). Myeloid neoplasms are heterogeneous clonal diseases of hematopoietic stem and progenitor cells, originate from mutations involving tumor suppressors, transcription factors, spliceosome components, epigenetic regulators, and, in particular, cohesin genes and proteins that control their function. Overall, these findings highlight the central role of NIPBL not only in embryonic development and chromatin organization, but also in the maintenance of normal hematopoiesis. Its alteration may therefore contribute to disease through mechanism involving transcriptional dysregulation and impaired cellular differentiation.

2.3 Role of Chromatin Disorganization and the Cohesin Complex in Leukemogenesis: Links Between Cornelia de Lange Syndrome and Acute Myeloid Leukemia.

Chromatin disorganization is increasingly recognized as a central element in the pathogenesis of myelodysplastic syndromes (MDS) and their progression to acute myeloid leukemia (AML). Alterations in genes encoding components of the cohesin genes (*STAG2, RAD21, SMC1A, SMC3, PDS5B*) or their regulators (including *NIPBL, MAU2, HDAC8*) have profound consequences on the biology of hematopoietic stem and progenitor cells, affecting the three-dimensional organization of the genome and transcriptional regulation.

Cornelia de Lange syndrome (CdLS), a prototypical chromatinopathy, is caused by mutations in cohesin-related genes. Interestingly, alterations in these the same genes are also observed in approximately one-fifth of patients with normal karyotype AML, frequently in association with mutations in *NPM1, FLT3, RUNX1, and ASXL1*.

Acute myeloid leukemis is a highly heterogeneous disease characterized by the accumulation of immature myeloid cells resulting from a combined disruption of proliferation and differentiation processes. According to the "two-hit" model, leukemogenesis requires the cooperation of class I mutations, which promote cellular proliferation (e.g., *FLT3* and *RAS*), and class II mutations, which impair hematopoietic differentiation (e.g., *NPM1* and *CEBPA*). More recently, a third class of alterations involving epigenetic regulators has been identified, highlighting the crucial role of chromatin in leukemogenesis (De Kouchkovsky e Abdul-Hay, 2016). In this context, alterations affecting the cohesion complex can be interpreted as mechanisms contributing to transcriptional dysregulation and the maintenance of a progenitor-like state, acting in synergy with oncogenic mutations that promote cell proliferation and survival. Notably, somatic mutations in cohesin genes have been identified in a significant proportion of myeloid malignancies, including AML and myelodysplastic syndromes, suggesting that they may act as driver events rather secondary alterations in tumorigenesis (Rigotti *et al.*, 2025). The relevance of epigenetic dysregulation in leukemogenesis is supported by the involvement of genes such as *KMT2A* (*MLL1*), a lysine methyltransferase responsible for histone H3 lysine 4 (H3K4) methylation, a key mark associated with transcriptional activation. Somatic mutations in *KMT2A* are frequently observed in hematologic malignancies, while germline variants have been associated with several chromatinopathies, including CdLS, highlighting an overlap between developmental disorders and cancer (Castiglioni *et al.*, 2022).

Based on the accumulated results described above, experimental evidence derived from induced pluripotent stem cell (iPSC) line may provide additional insights into these mechanisms. An iPSC line was generated in the Molecular Biology Laboratory from a CdLS patient carrying a heterozygous missense mutation in NIPBL (5483G>A; Arg1828Gln), together with isogenic corrected lines and healthy parental controls. Differentiation studies using those iPSC lines, demonstrated that impaired hepatic maturation associated with gene silencing (*DPP6*, *ZNF* gene cluster), which are linked to closed chromatin conformation and promoter methylation (Foglia, sine data). In addition, the differentiation of CdLS patient derived iPSC along neuronal cell lineage is defective in the maturation of cortical neurons and its mechanism seem to be senescence and apoptosis (Foglia M, unpublished results).

These findings are consistent with the biological features of AML, which is characterized by a block in differentiation combined with uncontrolled proliferation. At the molecular level, such alterations are associated with changes in chromatin accessibility, promoter methylation, and gene expression, affecting key pathways involved in cell fate determination (De Kouchkovsky e Abdul-Hay, 2016).

Mutations in *FLT3* and *NPM1* represent some of the most frequent molecular alterations in normal karyotype AML and play a critical role in disease pathogenesis and patient prognostic stratification. The *FLT3* gene encodes a receptor tyrosine kinase expressed in hematopoietic progenitor cells and is involved in cellular proliferation, survival, and differentiation. Activating mutations, such as internal tandem duplications (*FLT3-ITD*) or point mutations *(FLT3-D835*), lead to constitutive activation of signaling pathways and promote leukemogenesis. Similarly, mutations in the *NPM1* result in aberrant cytoplasmic localization of the protein, contributing to the dysregulation of tumor suppressor pathways (Yusoff *et al.*, 2019).

It is also noteworthy that alterations in cohesion-related genes been directly linked to hematological malignancies. Heterozygous mutations in *NIPBL* have been identified in pediatric cases B-cell precursor acute lymphoblastic leukemia (ALL) in pediatric patients, while reduced *NIPBL* expression promotes AML progression in the presence of *NPM1* mutations. In addition, decreased expression of *SMC1A* has been associated with poor prognosis in elderly AML patient.

Overall, these findings support the hypothesis that chromatin disorganization and alterations in cohesion function represent key drivers of leukemogenesis. Rather than acting solely as secondary events, these alterations contribute to the maintenance of an undifferentiated cellular state and to disruption of transcriptional programs that regulate normal hematopoiesis. In this context, cellular models derived from CdLS patients represent a valuable tool to investigate the molecular mechanisms underlying these alterations. Transcriptomic analysis, allow the identification of dysregulated biological pathways integrative approaches such as Gene Set Enrichment Analysis (GSEA) enable the interpretation of the changes at the level of biological networks.
In parallel, flow cytometry (FACS) provides functional validation by enabling the phenotypic characterization of cell populations and the identification of alterations in differentiation processes.

Therefore, the integration of genomic, transcriptomic, and phenotypic data represents a crucial approach to elucidate the contribution of chromatin alterations in the pathogenesis of hematologic malignancies and to identify potential novel therapeutic targets.

2.4 Study models for Cornelia de Lange Syndrome

Since the majority of individuals affected by Cornelia de Lange Syndrome (CdLS) present haploinsufficiency of the *NIPBL* gene, most of the experimental models developed to date have focused on investigating the consequences of altered NIPBL expression.
One of the earliest models organisms used to used CdLS was *Drosophila*, available since 1999 thanks to the work of Rollins et al., who employed morpholino oligonucleotides targeting the ATG regions of *NIPBL* in order to reduce its expression (Rollins, Morcillo e Dorsett, 1999).

Subsequently, transgenic murine models *Nipbl*+/− were developed. In these models, the insertion of "gene trap" cassettes allowed partial reduction of Nipbl expression, leading to phenotypes that recapitulate several features observed in CdLS patients, including cardiac, cerebral, and gastrointestinal malformations (Kawauchi *et al.*, 2009; KAWAUCHI *et al.*, 2016). These models have been particularly useful for studying the systemic effects of NIPBL haploinsufficiency in a mammalian context.

The zebrafish model was also widely used primarily through the application of morpholino oligonucleotides, capable of silencing *NIPBL* expression (Muto et al., 2011). In parallel, models based on human fibroblasts obtained from skin biopsies of patients have been developed (Fazio *et al.*, 2017) allowing the investigation of the disorder in a human cellular context.
These models allow the study of disease-related molecular alterations in a human context, although they are limited by their restricted differentiation potential and inability to fully recapitulate early developmental stages. Overall, these experimental systems have contributed significantly to understand the role of NIPBL and cohesion complex. However, they also present important limitations, including species-specific differences and the difficulty of modeling early embryonic development in controlled manner. In addition, the complex interactions between NIPBL, cohesin, accessory proteins, and transcriptional regulators remains only partially understood.

To overcome these difficulties, the use of induced pluripotent stem cells (iPSCs) has become increasingly relevant in recent years. iPSC can be generated from somatic cells, such as a peripheral blood mononuclear cell (PBMCs), through reprogramming techniques. These cells are subsequently validated through methods such as immunocytochemistry, immunofluorescence, and qRT-PCR in order to confirm the expression of pluripotency markers (Chen *et al.*, 2022; Li *et al.*, 2023).

A significant advancement in this field was provided by studies by (Mills *et al.*, 2018) in which iPSCs were differentiated into specific cell type like cardiomyocytes, to analyze the effects of *NIPBL* mutations both in the undifferentiated state and in differentiated cells. This approach allowed a deeper investigation of the role of the gene not only during embryonic development, but also in the functionality of specific tissues.

The introduction of iPSC-based models has therefore allowed researchers to overcome many of the limitations of traditional models, opening the way to a more precise characterization of the pathogenetic mechanisms of the syndrome, both during the different stages of embryogenesis and across various differentiated cell types (Mills *et al.*, 2018).

2.4.1 iPSCs and stem cells: general characteristics

Induced pluripotent stem cells (iPSCs) represent one of the most significant discoveries in modern biomedical research. They are derived from somatic cells that, through specific reprogramming strategies, are reverted to a pluripotent state, acquiring characteristics similar to those of embryonic stem cells.

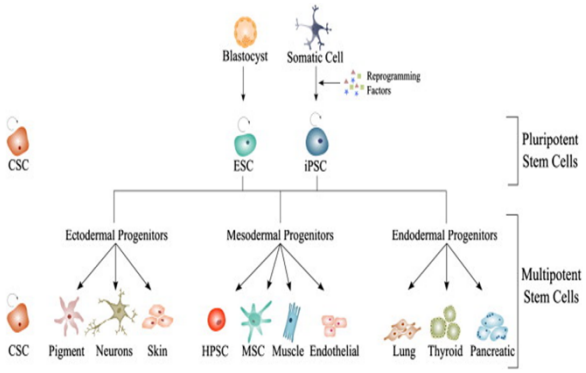

Figure 6. Differentiation of iPSc into various into lineage-committed cell-type (source: Creative Bioarray)

This technology was developed in 2006 by Shinya Yamanaka and Kazutoshi Takahashi, who demonstrated that the introduction of four transcription factors namely MYC, OCT3/4, SOX2, and KLF4 is sufficient to reprogram differentiated cells into pluripotent stem cells (Okita *et al.*, 2008). This discovery revolutionized the field of stem cell biology, providing an alternative to embryonic stem cells without the associated ethical concern.

Stem cells are distinguished by two fundamental properties: self-renewal, defined as the ability to replicate indefinitely while maintaining the same

degree of differentiation, and pluripotency, which refers to the capacity to generate multiple cell types through differentiation processes. Based on their differentiation potential, stem cells are classified as totipotent (capable of generating all cell types, including extraembryonic structures, such as the zygote in mammals), pluripotent (able to differentiate into the three embryonic germ layers but not into extraembryonic cells), multipotent (specialized in a limited number of cell types, for example hematopoietic stem cells), and unipotent (which can generate only a single cell type). The concept of the stem cell dates back to the end of the nineteenth century, but the first true characterization is attributed to experiments conducted in the 1960s by Ernest McCulloch and James Till at the University of Toronto and the Ontario Cancer Institute. Serendipitously, during studies on the effects of radiation in mice, the two scientists observed the formation of cellular colonies in the spleen of irradiated animals that had undergone bone marrow transplantation. These observations led them to hypothesize and subsequently demonstrate the existence of cells capable of self-renewal, a definition that remains at the basis of the modern concept of stemness.

In addition to classification based on differentiation potential, stem cells can also be categorized according to their origin. These include placental stem cells, chorionic villus stem cells, amniotic stem cells, hematopoietic stem cells derived from placental and cord blood, adult stem cells, embryonic stem cells (ESCs), and, more recently, iPSCs.

A peculiarity shared by all these cells is the ability to enter and exit the G0 phase of the cell cycle, thus maintaining an undifferentiated state and remaining ready to undergo differentiation following external stimuli (Nakamura-Ishizu, Takizawa e Suda, 2014).

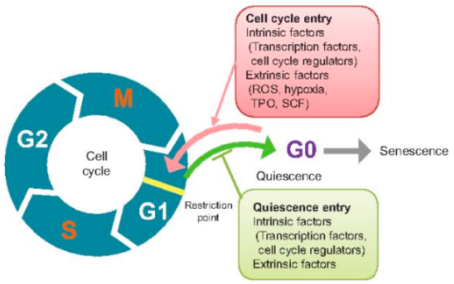

Figure 7. Stem cells also undergo the four phases of the cell cycle; once the restriction point is passed, they are able to divide, otherwise they remain in the quiescent G0 state (source: Nakamura et al., 2014).

Although iPSCs share many characteristics with embryonic stem cells (ESCs), they differ from them in important epigenetic aspects. In particular, in iPSC chromatin appears more methylated and less accessible, with significant consequences for the regulation of gene expression (Kimbrel e Lanza, 2016). For this reason, iPSCs are considered as an extraordinary resource for biomedical research, as they allow the study of genetic diseases without resorting to ethically controversial practices such as the destruction of embryos.

Historically, before Yamanaka's discovery, alternative and often complex methods had been developed to obtain pluripotent cells, such as Single Blastomere Technology (isolation of a single blastomere during the morula stage) or Somatic Cell Nuclear Transfer (SCNT), which involved replacing the nucleus of an oocyte with that of a somatic cell, leading to the development of pluripotent cellular clones (Kimbrel e Lanza, 2016). However, these approaches are now rarely used, having been replaced by the use of iPSCs, which have the major advantage of not requiring the use of embryonic cells.

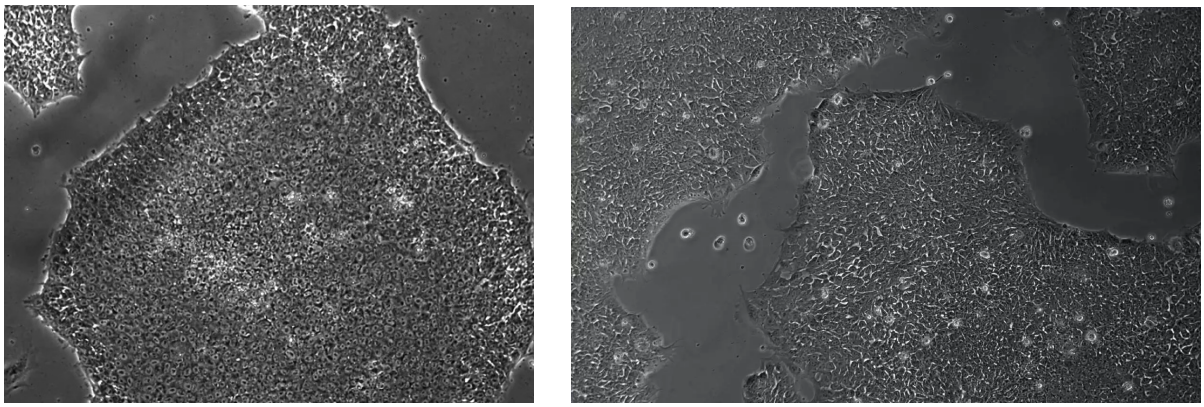

Figure 8. iPSC (source: ES/iPS cells (human) | Miltenyi Biotec | USA)

Numerous strategies have been developed over time to generate iPSCs. Among the most common are the use of viral vectors (lentivirus, adenovirus, Sendai virus) and non-viral approaches (mRNA/miRNA transfection, introduction of recombinant proteins, use of episomes). Each method presents advantages and limitations, and the choice depends on the experimental context and the therapeutic application (Lee *et al.*, 2009; Malik e Rao, 2013; Sommer *et al.*, sine data).
Once obtained, iPSCs must be carefully characterized. Conventional methods include karyotyping and histological analysis, which are useful to verify chromosomal stability and the correct identity of the cell line, aspects that are fundamental to ensure safety in clinical applications (MartinsTaylor e Xu, sine data a). More recent techniques, such as Teratoscore (Avior, Biancotti e Benvenisty, 2015), Pluritest (Müller *et al.*,

2011), and qPCR Scorecard (Tsankov *et al.*, 2015), allow quantitative and functional characterization of iPSCs by evaluating their differentiation capacity and distinguishing them from cellular populations that have lost pluripotency.

Finally, the analysis of telomeres and telomerase represents an additional useful tool to evaluate the stability and integrity of iPSC lines, parameters that are crucial for their application in therapeutic protocols (Liu, 2017). The evolution of analytical technologies, including ddPCR and microfluidic chip-based systems, contributes to further refining cell characterization and making their use increasingly safe within the framework of personalized medicine (MartinsTaylor e Xu, sine data b).

CHAPTER 3 - Materials and Methods

3.1 Reprogramming of iPSCs

The reprogramming of iPSC and sequencing were approved by the Regional Ethical Committee of Lombardy.

The reprogramming of peripheral blood mononuclear cells (PBMCs) into induced pluripotent stem cells (iPSCs) was performed using the CytoTune™ iPS 2.1 Sendai Reprogramming Kit (Invitrogen™). This system based on a modified, non-transmissible form of the Sendai virus, which allows efficient delivery of reprogramming factors without integration into host genome. The viral vectors are replication-defective and are progressively eliminated form transduced cells due to temperature-sensitive mutations.

PBMCs were isolated forma peripheral blood samples by density gradient centrifugation using Ficoll-Paque (Merck^{TM}). Following isolation, the cells obtained were subsequently cryopreserved in liquid nitrogen in a medium containing dimethyl sulfoxide (DMSO) and fetal bovine serum (FBS). Four days prior to reprogramming, PBMCs were cultured in 24-well plates at a density of 5×10^5 cells/mL in complete StemPro-34 medium supplemented with stem cells factor like SCF (100 ng/mL), FLT-3 (100 ng/mL), interleukin like IL-3 20 ng/mL, IL-6 (20 ng/mL) and L-glutamine (2 mM). cells were maintained under standard cuture conditions (37°C, 5% CO_2).

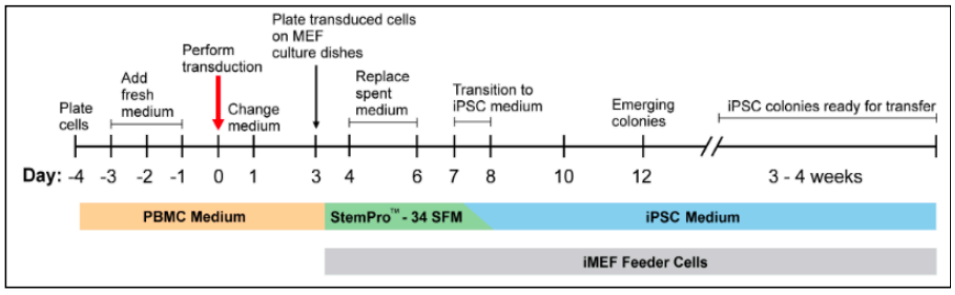

Figure 9. ***Reprogramming scheme starting from leukocytes*** *(source: Iborra-Egea et al., 2022).*

On day 0, PBMCs were transduced with the three vectors provided in the kit: KOS (containing the genes Klf4, Oct-4, Sox2), hc-Myc, and hKlf4. The multiplicity of infection (MOI) was adjusted according the manufacturer's recommendations, typically using MOI values of 5:5:3 for KOS, hc-Myc and hKlf4.

Component[1]	Cap color	Amount[2]		Storage
		A16517	A16518	
CytoTune™ 2.0 KOS	clear	100 µL	3 × 100 µL	–80°C
CytoTune™ 2.0 hc-Myc	white	100 µL	3 × 100 µL	
CytoTune™ 2.0 hKlf4	red	100 µL	3 × 100 µL	

$$\text{Volume of virus (µL)} = \frac{\text{MOI (CIU/cell)} \times \text{number of cells}}{\text{titer of virus (CIU/mL)} \times 10^{-3}\ \text{(mL/µL)}}$$

Figure 10. Components used for reprogramming and quantities (source: CytoTune-iPS 2.0 Sendai Reprogramming Kit | Thermo Fisher Scientific – IT)

After overnight incubation, the culture medium was replaced to remove residual vector, and the transduction-positive cells were subsequently seeded onto a Matrigel coating in the presence of StemPro-34 medium lacking cytokines but supplemented with L-glutamine (2 mM). Starting from day 7, the culture was maintained in a medium composed of 50% iPSC medium and 50% StemPro-34 without cytokines, with a final volume of 2 mL and daily medium replacement. The first cellular colonies, morphologically compatible with iPSCs, were observed between the seventh and the fourteenth day after transduction and characterized by in situ staining for the markers TRA-1-60 and TRA-1-81. Positive colonies were then transferred into 12- or 24-well plates previously treated with Attachment Factor to allow their expansion.

During the first 48 hours post-transduction, the cultures were constantly monitored under the microscope to evaluate the efficiency of transduction, cell mortality – which exceeds 60% – and the possible appearance of aggregates or morphological alterations. From day twenty-one, the colonies showed a more compact appearance and a progressive increase in size, eventually covering most of the plate surface. However, only a fraction of these corresponded to authentic iPSCs, distinguishable both by their morphology and by positivity for specific markers.

The derived clones were therefore used for the various experimental investigations planned or, alternatively, cryopreserved in vials in liquid nitrogen. For the latter procedure, two different freezing solutions were used: Freezing Medium A (composed of DMEM/F12 in a 1:1 ratio, 20% FCS, Rock Inhibitor Y-27632 1 µM; Miltenyi™) and Freezing Medium B (DMEM/F12 1:1, 20% FCS, 10% DMSO, Rock Inhibitor Y-27632 1 µM).

3.2 Maintenance of iPSC culture

Induced pluripotent stem cells (iPSCs) were cultured in 6-, 12-, or 24-well plates previously coated with Matrigel (Corning, Basement Membrane Matrix Growth Factor Reduced, Phenol Red Free) or with Geltrex (Invitrogen™). Culture conditions were set to preserve the

undifferentiated state and proliferative capacity of the cells, using the TeSR-E8™ proliferation medium (StemCell Technologies™) supplemented with 50X Supplement (StemCell Technologies™). Pluripotency was maintained by periodically isolating individual cellular clones from any differentiated cells and transferring them to new culture plates, based on the number and size of the clones present. This procedure was performed in the presence of medium containing Rock Inhibitor (Y-27632, 10 µM, StemMACS™), a GTPase inhibitor that reduces the risk of cellular differentiation during handling. Clone isolation was carried out under a horizontal laminar flow hood by observing the cells under an optical microscope (4X magnification). Selected clones were then carefully picked using a Gilson™ p200 micropipette, allowing gentle detachment of the colonies from the substrate and their transfer to new wells for expansion.

In addition to manual approach, an immunomagnetic selection system based on Anti-TRA-1-60 Microbeads (Miltenyi™) was employed. This method exploits the expression of the surface marker TRA-1-60, which is typically down-regulated during differentiation, to enrich the population of pluripotent cells. In this case, cells were initially detached by incubation with Accumax™ (Merck™) for 2–3 minutes at 37°C, and the reaction was subsequently stopped by adding DMEM containing 5% FCS and Rock Inhibitor (1 µM). Cells were then filtered through 30 µm filters and counted using a Bürker chamber in the presence of Trypan Blue (1:1) to assess viability. The cell suspension was loaded onto MS Columns (Miltenyi™), with a maximum of 2×10^6 cells per column. The protocol included centrifugation at 300 g for 5 minutes at room temperature, followed by resuspension of the pellet in 80 µL of TeSR-E8™ medium supplemented with Rock Inhibitor (10 µM, 1:1000), to which 20 µL of Anti-TRA-1-60 Microbeads were added. After a 5-minute incubation, the columns were equilibrated with 0.5 mL of the same medium, followed by sample loading and three washes with 0.5 mL of fresh medium. The enriched cells were then eluted using 1 mL of TeSR-E8™ containing Rock Inhibitor (10 µM) and recounted using a Bürker chamber. Cells were plated at densities proportional to the plate size, corresponding to 0.8×10^6 cells per well for 6-well plates.

Alternatively, cells were detached using Versene 1X (Gibco™) and a Cell Scraper (Corning™), then centrifuged at 300 g for 2 minutes in PBS 1X/DMEM. After aspirating the supernatant, the cell pellet was resuspended in 1 mL of PBS and subjected to an additional centrifugation at 4°C at maximum speed for 5 minutes. The final pellet obtained was used for subsequent experimental analyses.

3.3 RNA Extraction and RNA-seq Analysis

Total RNA, including small RNA species, was extracted using the miRNeasy Mini Kit (Qiagen, Hilden, Germany), following the manufacturer's instructions. Prior to the procedure, buffers RWT and RPE were prepared by adding ethanol (96–100%) as indicated. All steps were performed at room temperature (15–25°C), except for the phase separation step. Any precipitates present in buffer RWT were dissolved by heating.

For cell lysis, 700 µl of QIAzol® reagent was added to each sample, followed by homogenization using an appropriate method and incubation at room temperature for 5 minutes. Subsequently, 140 µl of chloroform was added, and samples were vigorously shaken for 15 seconds and incubated for an additional 2–3 minutes. Phase separation was achieved by centrifugation at 12,000 × g for 15 minutes at 4°C. The upper aqueous phase containing RNA was carefully transferred to a new tube, avoiding the interphase, and mixed with 1.5 volumes of 100% ethanol.

The resulting solution was loaded (up to 700 µl per step) onto an RNeasy column placed in a 2 ml collection tube and centrifuged at ≥8000 × g for 15 seconds. The flow-through was discarded, and the step was repeated until the entire sample had been processed. When required, DNase digestion was performed according to the manufacturer's instructions to remove genomic DNA contamination (optional step). The column was then washed with 700 µl of buffer RWT and centrifuged at ≥8000 × g for 15 seconds (this step may be omitted when working with cultured cells). Two additional washes were performed with buffer RPE (500 µl each), followed by centrifugation for 15 seconds and 2 minutes, respectively, at ≥8000 × g. To remove residual ethanol, the column was centrifuged at full speed for 1 minute (optional step). RNA was eluted by transferring the column to a new 1.5 ml tube and adding 30–50 µl of RNase-free water directly onto the membrane, followed by centrifugation at ≥8000 × g for 1 minute. In cases of high RNA yield (>30 µg), elution was repeated to increase RNA concentration.

RNA sequencing was performed using the Illumina NextSeq500 platform, generating paired-end reads of 121 base pairs in length. The quality of sequencing reads was assessed using FastQC (version 0.11.9).
Strand-specific total RNA reads were aligned to the human reference genome (GRCh38) using STAR (version 2.7.11b) in two-pass mode. Gene expression quantification was performed at the gene level using comprehensive annotations from Gencode (release hg38.v38, GTF file).
Data were normalized according to library size and subjected to variance stabilizing transformation (vst) in the R statistical environment.

Differential expression analysis was carried out using the DESeq2 package (version 1.46.0).
Gene set enrichment analysis was performed using the limma package (version 3.62.2), employing gene collections derived from the Molecular Signatures Database (MSigDB). P-values were adjusted for multiple testing using the false discovery rate (FDR), with a significance threshold set at 0.05.

Gene Set Enrichment Analysis (GSEA) was subsequently conducted using the ClusterProfiler package (version 4.14.6) in R, applying the fgsea algorithm. Genes were ranked based on a signed significance metric, defined as the product of the negative log10-transformed p-value and the sign of the log2 fold change. Gene set definitions were obtained from MSigDB in .gmt format.
For each gene set, the normalized enrichment score (NES), nominal p-values, and FDR q-values were calculated, considering gene sets with q-values < 0.05 as significantly enriched.

GSEA results were visualized using Cytoscape (version 3.10.1) with the EnrichmentMap application. Enrichment maps were generated using a node significance threshold of q-value ≤ 0.10 and an edge similarity threshold of 0.375. In the resulting network, each node represents a gene set enriched in at least one of the analyzed conditions or comparisons. For each node, an embedded pie chart summarizes enrichment across conditions, with each slice corresponding to a specific comparison. Slice color reflects the NES value: positive values are shown in red, negative values in blue, and non-significant enrichments in grey. Node size is proportional to the number of genes within the set.
Edges represent the degree of overlap between gene sets, with thickness and color intensity proportional to the extent of gene sharing. Pathways of interest were finally selected and grouped into broader functional categories through manual inspection of individual gene sets and their biological annotations.

3.4 STEMdiff™ Monocyte kit

The differentiation of induced pluripotent stem (iPS) cells into monocytes was performed using the STEMdiff™ Monocyte Kit (STEMCELL Technologies), according to the manufacturer's instructions. iPS cells were maintained in TeSR-E8 medium and subsequently dissociated to obtain cell aggregates with a diameter ranging from 100 to 200 µm. Aggregates were then seeded onto Geltrex-coated 6-well plates at a density of approximately 100–200 aggregates per well (corresponding to ~10–20 aggregates/cm²) in 2 mL of maintenance medium. Cells were

incubated at 37°C in a humidified atmosphere containing 5% CO_2 and allowed to adhere for 24 hours without disturbance.

The differentiation protocol was carried out in three sequential stages. During stage 1 (days 0–3)**,** aimed at mesoderm induction, the maintenance medium was replaced with 2.5 mL of Medium A, consisting of hematopoietic basal medium supplemented with STEMdiff™ Hematopoietic Supplement A. After 48 hours, a partial medium change was performed by removing 1.25 mL and replacing it with an equal volume of fresh Medium A, followed by an additional 24 hours of incubation.

During stage 2 (days 3–7)**,** aimed at hematopoietic differentiation, the culture medium was completely replaced with 2.5 mL of Medium B, consisting of hematopoietic basal medium supplemented with STEMdiff™ Hematopoietic Supplement B. After 48 hours, a further partial medium change was performed by removing 1.25 mL and adding an equal volume of fresh Medium B, followed by incubation for an additional two days.

From day 7 onward (stage 3)**,** cells were cultured in Monocyte Differentiation Medium, consisting of StemSpan™ SFEM II supplemented with STEMdiff™ Monocyte Differentiation Supplement, to promote maturation into monocytes. The medium was completely replaced with 2 mL per well and refreshed every 2–3 days throughout the culture period. During this stage, the progressive appearance of non-adherent cells in the supernatant was observed, indicating monocyte formation.

From day 14**,** monocytes were collected from the culture supernatant. The medium containing the cells was harvested and used to resuspend any partially adherent cells, then transferred to centrifuge tubes and centrifuged at 300 × g for 5 minutes at room temperature. The supernatant was discarded, and the cell pellet was resuspended in the appropriate medium for downstream analyses.

Monocyte collection was performed every 2–3 days; alternatively, complete medium changes were carried out to maintain the culture. Peak production of $CD14^+$ monocytes was observed between days 17 and 22, with a reported frequency of approximately 60–80%. To increase cell yield, the volume of medium added could be increased or the interval between medium changes extended to allow cell accumulation in the supernatant.

.

3.5 Protocol for differentiation of monocytes and macrophages from human induced pluripotent stem cells.

The analysis of immune cells in Cornelia de Lange syndrome, particularly monocytes and macrophages, is hindered by the limited availability of primary tissues; however, this limitation can be overcome through the use of human induced pluripotent stem cell (iPSC) technology. The protocol used, namely "Protocol for differentiation of monocytes and macrophages from human induced pluripotent stem cells" from Cell Press, allows the differentiation of myeloid lineage cells from human iPSCs obtained from multiple donors (Emmerich, sine data). An extensive characterization was performed on the cell lines that consistently produced the highest number of floating hematopoietic progenitor cells (HPCs), monocytes, and macrophages. All cells were cultured in standard incubators at 37 C (5% CO2, 20% O2) and all medium changes/non-terminal characterization steps were performed in sterile conditions. The process of differentiating iPSCs into myeloid lineage cells involves a sequence of progressive stages. Initially, the cells acquire characteristics of mesoderm progenitor cells, followed by the formation of monolayered HPCs. Subsequently, the cells differentiate into myeloid progenitors, which mature into monocytes. Finally, these monocytes develop into macrophages, which can adopt polarized M1 or M2 phenotypes depending on the experimental conditions.

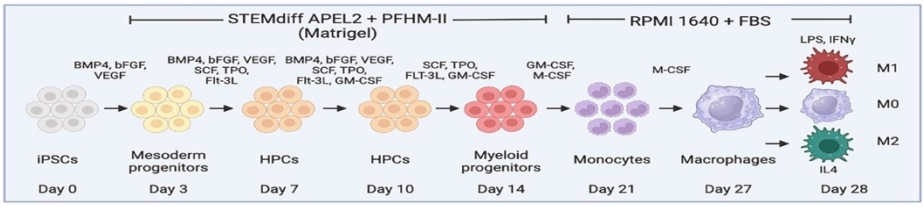

Figure 11. ***Differentiation timeline of hiPSCs into myeloid lineage cells****. hiPSCs form small colonies and are treated with growth factors to induce mesoderm progenitors (days 0–3), hematopoietic progenitors (HPCs, days 3–7), and proliferating HPCs (days 7–10). From days 10–14, floating myeloid progenitors develop, replated on low-attachment plates and treated to produce monocytes and mature myeloid cells (days 14–21). Monocytes can further mature into resting M0 macrophages (days 21–28) and be polarized into M1 or M2 macrophages after 24 h of additional treatment. Source: Emmerich et al.*

3.5.1 From day -1 to day 0: hiPSC passaging during the pre-differentiation phase

Undifferentiated iPSCs were maintained through regular passaging every 3–4 days upon reaching approximately 80% confluency, using split ratios ranging from 1:5 to 1:10 in order to preserve pluripotency. The culture

medium (TeSR-E8) was refreshed daily to prevent spontaneous differentiation prior to cell passaging.
To initiate differentiation, cells were passaged under standard conditions and subsequently seeded onto plates previously coated with Geltrex. Upon reaching 80% confluency, the culture medium was removed, cells were washed with DPBS, and then treated with Versene to promote detachment. After incubation for 5 minutes at 37 °C, cells were gently resuspended in TeSR-E8 medium and transferred into new wells containing TeSR-E8 supplemented with ROCK inhibitor.
Cells were then seeded at a 1:100 split ratio, ensuring homogeneous distribution within the wells, and incubated overnight at 37 °C. The following day (day 0), the differentiation process was initiated by adding the specific medium for mesoderm induction.
Particular attention was given to cell density and colony size prior to the initiation of differentiation, as these parameters were found to be critical for the proper execution of the protocol. In particular, a 1:100 split ratio from cultures at 80% confluency proved to be optimal.

3.5.2 From day 0 to day 3: mesoderm induction

Mesoderm induction represents the first step of the differentiation process and is aimed at generating mesoderm lineage cells, which can subsequently be directed toward hematopoietic progenitor cells. Starting from the small colonies obtained after iPSC passaging, cell clusters progressively increase in size throughout this stage. Day 0 is defined as the beginning of the differentiation process.

The mesoderm induction medium for the early stages of differentiation was prepared as follows: the basal early-stage differentiation medium consisted of STEMdiff APEL 2 medium supplemented with 5% Protein-Free Hybridoma Medium (PFHM-II), to which specific growth factors and reagents were added, including BMP4 (10 ng/mL), VEGF (10 ng/mL), and FGF (10 ng/mL). Prior to use, the prepared medium was sterilized by filtration through a 0.22 μm filter.

On day 0, the TeSR-E8 medium with Rock 10μM from the previous day was gently aspirated and replaced with 1.5 mL of mesoderm induction medium; cells were then incubated at 37 °C until day 2. At this time point, the medium was removed and replaced with 1.5 mL of fresh mesoderm induction medium.

3.5.3 From day 3 to day 10: HPC commitment and expansion

The second stage of the differentiation process is aimed at committing cells toward the hematopoietic lineage. During the early phase (days 3–7), the monolayer culture exhibits significant growth, in some cases reaching near confluency. In the later phase (days 7–10), hematopoietic progenitor cells (HPCs) begin to appear, characterized by a floating morphology above the adherent monolayer.
For this stage, two distinct media were employed: the first to promote HPC commitment and the second to support their expansion. It is important to note that, at this stage, variability among different cell lines may become evident in terms of timing and efficiency of HPC generation. In highly efficient differentiating lines, floating cells are typically observed between days 8 and 10, whereas in other lines they may still be absent at the same time point.

On day 3, the mesoderm induction medium was removed and replaced with HPC commitment medium, consisting of basal early-stage differentiation medium supplemented with growth factors including BMP4 (10 ng/mL), VEGF (10 ng/mL), bFGF (10 ng/mL), SCF, (50 ng/mL), TPO (50 ng/mL), and FLT-3 (50 ng/mL). Cells were then incubated at 37 °C until day 5. The medium was subsequently refreshed and maintained until day 7, when cultures were examined under a microscope to assess the presence of floating HPCs.
From day 7 onward, the medium was replaced with HPC expansion medium, based on basal early-stage differentiation medium and further supplemented with BMP4 (10 ng/mL), VEGF (10 ng/mL),, bFGF (10 ng/mL), SCF (50 ng/mL), TPO (50 ng/mL), FLT-3 (10 ng/mL), and GM-CSF (100 ng/mL), in order to promote HPC proliferation. Cells were incubated until day 9, with an additional medium change performed during this period.
On day 10, floating Myeloid Progenitor cells (MPCs) were collected by gently swirling the plate, transferred into conical tubes, and centrifuged at 600 g for 3 minutes at room temperature. Following washing with DPBS, cells were counted and seeded into new culture plates at appropriate densities.
The adherent monolayer cells were maintained separately in culture, allowing for subsequent collections of floating MPCs over time. Particular attention was given to the handling of MPCs from day 10 onward, as transferring them to new plates at optimal densities was found to enhance both their proliferation and their progressive commitment toward the myeloid lineage.

3.5.4 From day 10 to day 14: Myeloid lineage induction

This stage of the differentiation process is aimed at inducing floating MPCs to differentiate into myeloid lineage-committed cells. Following collection and seeding at the recommended densities, MPCs proliferate while predominantly remaining in small clusters or as single cells.
At this stage, HPCs previously associated with the monolayer are ideally collected and replated at the appropriate density. However, the adherent monolayer culture is maintained using the same medium as for the resuspended HPCs, allowing for the continuous collection of additional MPC populations that may emerge over time.
The basal medium for the late stages of differentiation (basal late-stage differentiation medium) consists of RPMI 1640 supplemented with 10% fetal bovine serum (FBS). This medium is further supplemented with growth factors including SCF (50 ng/mL), TPO (50 ng/mL), FLT-3L (50 ng/mL), and GM-CSF (100 ng/mL), to promote myeloid lineage induction.

On day 10, both monolayer cells and isolated MPC were cultured in myeloid induction medium. Specifically, the monolayer medium was replaced with 2 mL of fresh medium, while MPCs were seeded in the appropriate volume based on cell density. Cultures were then incubated at 37 °C until day 12.

On day 12, monolayer HPC cultures were examined under a microscope to assess the presence of additional floating MPC. If present, these were collected following the same procedure described in the previous stage and combined with the previously isolated HPCs. In the absence of newly formed MPCs, the monolayer medium was simply refreshed while maintaining the same volume. In most cell lines, the production of floating MPCs continues until day 14, making it advisable to maintain the culture beyond day 12 even in the absence of additional collections.
For isolated MPCs, medium renewal was performed by collecting the suspension cells into conical tubes, centrifuging at 600 g for 3 minutes at room temperature, and subsequently resuspending the cells in the same volume of myeloid induction medium. Cells were then replated into the original culture plate and incubated until day 14.

On day 14, cultures were again analyzed to determine the presence of additional floating MPCs, which, if present, were collected and pooled with previously harvested cells. This typically represents the final collection time point for HPCs in the tested cell lines.

HPCs collected at different time points (days 10, 12, and 14) were subjected to phenotypic characterization by flow cytometric analysis of CD34 and CD45 marker expression. For each analysis, at least 20,000 cells were used, including negative controls consisting of unstained cells

and, where possible, isotype controls. In efficiently differentiating cell lines, expression levels of approximately 85% for CD34 and 90% for CD45 were observed.

For flow cytometry sample preparation, MPCs were collected from the non-adherent plate, centrifuged at 600 g for 3 minutes, and resuspended in DPBS. Following optional cell counting, cells were centrifuged again and resuspended in a reduced volume of buffer, then incubated with CD34- and CD45-specific antibodies at concentrations recommended by the manufacturer for 30 minutes at 4 °C. Negative controls included isotype antibodies or fluorescence minus one (FMO) control. After incubation, cells were washed with DPBS, centrifuged, and resuspended in MACS buffer (PBS containing BSA and EDTA), and subsequently analyzed by flow cytometry according to the manufacturer's instructions.

3.5.5 From day 14 to day 21: monocyte formation

Following HPC generation, the protocol proceeded with a stage aimed at the maturation of myeloid cells, in particular the formation of monocytes. During this phase, differentiating cells increased in size and tended to form aggregates at the bottom of low-attachment plates. Variability in maturation timing was observed across different cell lines; therefore, the assessment of CD45, CD11b, and CD144 expression was used to determine the optimal timing for progression to downstream stages. The overall yield of iPSC-derived monocytes varied among cell lines and correlated with differentiation efficiency: highly efficient lines produced between 12 and 18 million cells from two wells of a 6-well plate, whereas less efficient lines yielded between 0.5 and 5 million cells.

The monocyte formation medium was prepared using basal late-stage medium consisting of RPMI supplemented with fetal bovine serum (FBS), to which the growth factors GM-CSF (100 ng/mL) and M-CSF (100 ng/mL) were added. Cells were collected from the myeloid lineage induction medium, centrifuged at 600 g for 3 minutes, resuspended in monocyte formation medium, and transferred to a new plate containing the appropriate volume of medium. Cultures were incubated at 37 °C until day 16. At this point, half of the medium was carefully removed to avoid cell loss and replaced with fresh medium; if cells did not appear adherent, they were collected, centrifuged, and replated. Medium refreshment was subsequently performed on days 18 and 20 following the same procedure. At this stage of differentiation, phenotypic characterization was performed by flow cytometric analysis of the pan-leukocyte marker CD45, the mature myeloid marker CD11b, and the monocyte marker CD14. This analysis was carried out between days 20 and 22, when efficiently differentiating cell lines exhibited expression levels of approximately 90% for CD45 and

CD11b and 80% for CD14, comparable to those observed in primary PBMC-derived monocytes. At this stage, the majority of cells appeared fully or partially attached to the bottom of the culture plate, thus requiring chemical dissociation for cell collection.

For flow cytometry sample preparation, the culture medium was carefully aspirated to retain adherent cells. An appropriate volume of Accutase (e.g., 1 mL per well of a 6-well plate or 4 mL for a 10 cm dish) was added, and cells were incubated at 37 °C for 5 minutes to promote detachment. Subsequently, a double volume of DMEM supplemented with 10% fetal bovine serum (FBS) was added, and cells were resuspended by pipetting and collected into 15 mL conical tubes. After centrifugation at 600 g for 3 minutes, the supernatant was removed and cells were resuspended in PBS. Following optional cell counting, cells were brought to a single-cell suspension, transferred to the appropriate volume into 1.5 mL Eppendorf tubes, and centrifuged again at 600 g for 3 minutes. The medium was then aspirated and replaced with 50 µL of PBS.
Cells were incubated with CD45-, CD11b-, and CD14-specific antibodies at concentrations recommended by the manufacturer for 30 minutes at 4 °C. To define the positivity threshold, negative controls including isotype antibodies or fluorescence minus one (FMO) controls were used for each analyzed marker. After incubation, PBS was added and cells were centrifuged at 600 g for 3 minutes; the supernatant was discarded and cells were resuspended in MACS buffer (PBS supplemented with BSA and EDTA).

3.5.6 From day 21 to day 28: macrophage production and polarization

The macrophage production and polarization stage was carried out between days 21 and 28 of the differentiation protocol, with a total duration of approximately 8 days. Following the generation of monocytes, this stage was aimed at their further differentiation into mature macrophages. The resulting macrophages were subsequently polarized from the basal M0 state into either M1 or M2 phenotypes in order to investigate different aspects of inflammatory responses.
The basal macrophage M0 medium was prepared as described in the Materials and Methods section. Cells from the previous stage were collected, centrifuged at 600 g for 3 minutes, and resuspended in basal M0 medium. The cells were then transferred to a new plate containing the appropriate volume of medium and incubated at 37 °C until day 23. Medium renewal was performed on days 23 and 25 by carefully removing half of the supernatant and replacing it with fresh basal M0 medium.
At day 27, cells were subjected to polarization toward M1 or M2 phenotypes. Polarization media were prepared as described in the

Materials and Methods section. Cells were collected and centrifuged at 600 g for 3 minutes; if cells were adherent, they were detached using Accutase. Following centrifugation, the cell pellet was resuspended in M1 or M2 polarization medium and transferred to a new plate containing the appropriate volume of the same medium. Cells were then incubated at 37 °C for 24 hours.

3.6 Immunofluorescence Analysis

Immunofluorescence analysis was employed to evaluate the expression and localization of specific protein markers associated with macrophage differentiation and polarization states. This technique allows the identification of distinct cellular phenotypes based on the detection of lineage-specific and activation-related antigens, such as CD68, CD80, and CD209, which are commonly used to characterize macrophage subsets. The method is based on the specific interaction between an antigen and its corresponding antibody. Primary antibodies selectively bind to target proteins expressed within the cells, while fluorophore-conjugated secondary antibodies recognize the primary antibodies and enable signal amplification. Upon excitation at specific wavelengths, the fluorophores emit light at defined emission spectra, allowing visualization of the target proteins using fluorescence microscopy.

In this study, immunofluorescence was particularly useful to assess differences between CdLS-derived and control cells across different macrophage polarization states (M0, M1, and M2). The use of multiple markers enabled the discrimination between general macrophage identity (CD68), pro-inflammatory phenotype (CD80), and anti-inflammatory phenotype (CD209), thereby providing insight into potential alterations in differentiation and functional polarization.

Furthermore, this technique allows not only qualitative evaluation but also spatial analysis of protein localization within the cellular context, offering additional information on cellular organization and functional status. Therefore, immunofluorescence represents a powerful tool to investigate phenotypic and functional differences associated with chromatin dysregulation in CdLS models.

For immunofluorescence analysis, cells were seeded onto glass coverslips (Hatfield, PA) previously treated with 50 µg/mL poly-L-ornithine and subsequently coated with Geltrex. Both iPSCs and differentiated cells were fixed using 2% formalin.

Following fixation, cells were incubated overnight at 4 °C with primary antibodies diluted in an incubation buffer containing 1× PBS, 1% BSA,

2% normal goat serum, and 0.1% Triton X-100. Cells were then incubated with the appropriate secondary antibodies for 1 hour at room temperature. After removal of the secondary antibodies, nuclei were stained with Hoechst dye for 2 minutes. Samples were mounted using ProLong Diamond mounting medium (Invitrogen, Waltham, MA), and fluorescence images were acquired using an Olympus IX71 microscope.

For the immunofluorescence characterization of macrophage populations, cells derived from Cornelia de Lange syndrome patients (MNCdLS) and healthy controls (MNMo1 and MNFa1) were analyzed at different stages of macrophage differentiation: M0 (unpolarized), M1 (pro-inflammatory phenotype), and M2 (anti-inflammatory phenotype). Specifically, the following experimental groups were included: MNCdLS M0, MNCdLS M1, MNCdLS M2, MNFa1 M0, MNFa1 M1, and MNFa1 M2.

Cells were processed according to the immunofluorescence protocol described above. After fixation and permeabilization, samples were incubated overnight at 4 °C with primary antibodies diluted in the incubation buffer. The following primary antibodies were used: anti-CD68 (Cell Signaling Technology, rabbit, 1:400), anti-CD80 (Abcam, rabbit, 1:100), and anti-CD209 (Bio-Rad, mouse, 1:100). After appropriate washing steps, cells were incubated for 1 hour at room temperature with the corresponding secondary antibodies: anti-rabbit conjugated to Alexa Fluor 546 and anti-mouse conjugated to Alexa Fluor 488.

3.7 Flow cytometry and FACS analysis

Flow Cytometry is a powerful technique used to analyze the physical and molecular characteristics of cells in suspension. A specific application of this method is fluorescence-activated cell sorting (FACS), which allows both the identification and physical separation of distinct cell populations based on fluorescent labeling.
Cells are first incubated with fluorochrome-conjugated antibodies directed against specific surface or intracellular markers, thus allowing, in this case, the distinction between stem cells, monocytes, and macrophages. The labeled cell suspension is then passed through a fluidic system in which cells flow individually through a laser beam. As each cell intercepts the laser, it scatters light and emits fluorescence signals that are detected by photodetectors.
Forward scatter (FSC) provides information regarding cell size, whereas side scatter (SSC) reflects cellular complexity or granularity. Fluorescence signals instead correspond to the expression of specific markers.
These signals are processed and analyzed to identify different cell populations. In FACS applications, cells can be electrostatically charged and physically sorted into separate containers according to their

fluorescence profile. This technique is widely used to characterize cell populations, quantify marker expression, and evaluate differentiation processes.

In the context of this study, flow cytometry represented a fundamental tool for evaluating the phenotypic properties of hematopoietic cells derived from induced pluripotent stem cells. This was made possible through the use of several specific antibodies, including TRA-1-60, required for the identification of human pluripotent stem cells; CD34, used for the recognition of hematopoietic stem cells; CD45, a pan-leukocyte marker expressed in hematopoietic cells; CD14 and CD11b, specific for monocytes and macrophages; and lastly, CD38.

The latter represents a particularly interesting marker because it was initially identified as a surface activation marker in lymphocytes; however, more recent studies have demonstrated that it is selectively upregulated in macrophages under inflammatory conditions (Guerau-de-Arellano, 2018).

CHAPTER 4 – RESULTS

4.1 Characterization of IPSC in this study

In order to evaluate the effect of the NIPBL mutation on hematopoietic differentiation, iPSC lines derived from the patient and the corresponding controls were differentiated along the myeloid lineage, according to the protocol described in the Materials and Methods section.

The project underlying this thesis is part of a broader study aimed at using induced pluripotent stem cells (iPSCs) as a model to identify the molecular mechanisms responsible for Cornelia de Lange Syndrome (CdLS). In this section, both the results obtained during the present work and the preliminary data generated by other members of the Molecular Biology laboratory are presented.
Peripheral blood mononuclear cells (PBMCs) isolated from the patient and her parents, used as healthy controls due to their shared genetic background, were reprogrammed using the Sendai virus to generate iPSCs. Successful reprogramming was confirmed both by the typical colony morphology and by the expression of stem cell markers OCT4A, TRA1-60, SOX2 and LIN28 assessed by immunofluorescence.
DNA sequencing further demonstrated that, following reprogramming, patient-derived iPSCs retained the mutation in the NIPBL gene (5483 G>A; Arg1828Gln) and did not present structural genomic alterations, such as deletions, duplications, or translocations, as shown by shallow whole genome sequencing analysis. As an additional control, an isogenic line in which the mutation was corrected using CRISPR/Cas9 technology (Umbach *et al.*, 2022) was employed.
RNA sequencing and Western blot analyses showed that the point mutation in the NIPBL gene does not significantly affect its expression nor that of other genes encoding components of the cohesin complex (SMC1, SMC3, RAD21, HDAC8, ANKRD11). However, transcriptomic analysis revealed the presence of numerous differentially expressed genes between the patient and control samples, involved in key biological processes related to the development of various organs, including the nervous system, liver, and kidney.
Based on these findings, the differentiation capacity of iPSCs toward different cellular lineages, including hepatic and neuronal lineages, was evaluated *in vitro*, highlighting differentiation defects in the mutated cells. Considering the known role of NIPBL and the cohesin complex in transcriptional regulation and chromatin organization, particularly in the formation of topologically associated domains (TADs), the study was further extended to investigate chromatin remodeling processes using techniques such as ATAC-seq and ChIP-seq. The results obtained

demonstrated that the deficits observed in the patient derived undifferentiated and differentiated iPSCs are likely to be due to a transcriptional dysregulation resulting from a cohesion-dependent alteration of chromatin accessibility.

4.2 Hematopoiesis using commercially available Kit

The initial hematopoietic differentiation experiment was performed using a commercially available kit, the protocol of which is described in the following section.

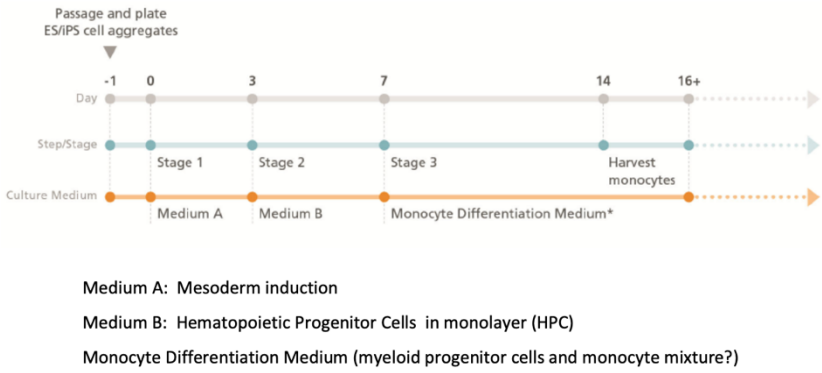

Figure 12. Commercially Available kit for differentiation in monocytes.

Time frame of the commercially available Kit is quite short and the good amounts of Monocytes started to be produced in 2 weeks. The differentiation status was monitored by FACS analysis, and the results are shown in Fig.13. Mature monocyte specific populations are defined by CD34-/CD45+/CD11b+/CD14+. As is shown in Figure 13, both the CdLS patient-derived iPSC (MNCdLS1) and the control iPSC derived from her healthy mother (MNMo1) are capable of producing monocytes defined by the specific cell surface antigen expression at day 19. However, the efficiency of Monocyte production of the hematopoietic progenitor cells derived from the patient iPSC at day14 is inferior to the control cells. In addition, the control iPSC produces normal round shape monocytes with approximately 20 micron in diameter, while the patient-derived monocytes very in size and some of them seem to be abnormal.

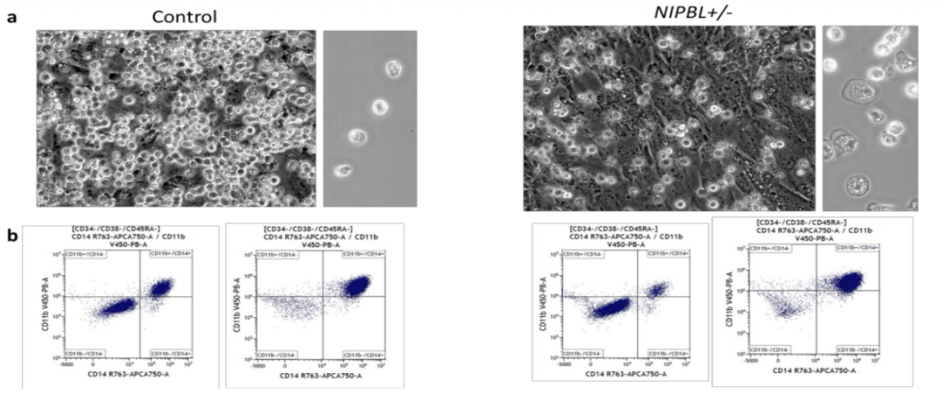

Figure 13. ***Differentiation of iPSCs (Tra-1-60+) with heterozygous NIPBL gene mutation (NIPBL+/-) and the respective control cells (control) along myeloid hematopoietic cells.***
a) The morphology of myeloid progenitor cells derived from CD34+/CD45+ hematopoietic stem cells, at day 14 on the left panel, and the floating monocytes at day 19 on the right panel.
b) FACS analysis was performed on the myeloid progenitor cells (left) and the floating monocytes (right) at day 19 differentiation. The CD11b+/CD14+ and CD11b-/CD14- cell populations are shown.

These preliminary findings suggest a potential impairment in the differentiation process of patient-derived iPSCs relative to control cells. Under physiological conditions, hematopoietic progenitor cells (HPCs) give rise to myeloid progenitor cells (MPCs), which subsequently differentiate into mature monocytes. However, the commercially available protocol does not allow a clear distinction between these populations, as the final product consists of a mixed population of HPCs and MPCs.
For this reason, the differentiation protocol was modified, as described in Section 5.3.

4.3 Diffentiation of iPSC along myeloid cell lineages

The protocol followed in the subsequent experiments is described below.

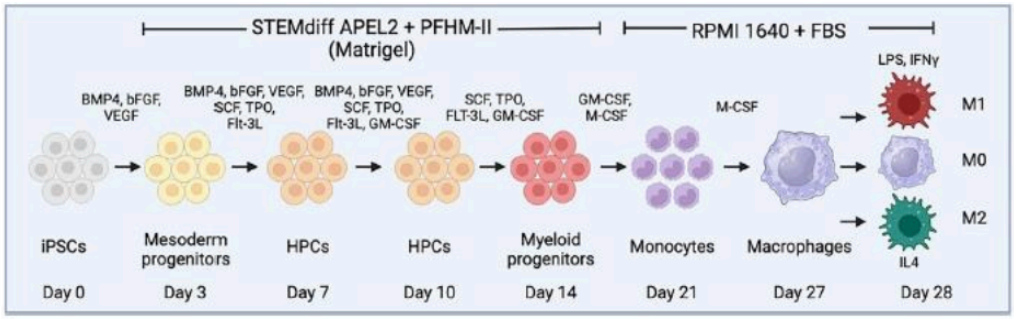

The differentiation process lasts approximately 25 days, during which a progressive emergence of different cell populations belonging to the myeloid lineage can be observed. In particular, monolayered hematopoietic progenitor cells (HPCs), which are committed to the hematopoietic lineage but still retain multipotent potential, are initially

generated. The HPCs started to produce floating myeloid progenitor cells (MPCs), which represent a more differentiated stage already committed to the myeloid lineage. The isolated MPCs can be subsequently differentiated into monocytes, which can further be transformed into macrophages. Those macrophages are capable to be polarized in M1 or M2 dependent upon appropriate stimuli. During the early stages of differentiation, differences between the cell lines were observed as early as day −1, at the time of iPSC replating. In particular, cells from the MNCdLS1 line exhibited reduced adhesion capacity, tending to detach and remain in suspension, making it difficult to achieve an optimal cell density. Despite this, the differentiation protocol was carried out.

Throughout the differentiation process, a similar progression of the monolayer was observed among the different cell lines. However, the production of hematopoietic progenitor cells (HPCs) in the CdLS-derived line was delayed. Specifically, the emergence of HPCs was observed around day 14, but in lower numbers compared to the control cells.

As indicated in Section I, the advantage of the second protocol lies in its ability to distinguish between myeloid progenitors and monocytes. Up to the stage of monocyte production, the identity of the different cell populations was characterized by FACS analysis, whereas the transition from monocytes to macrophages was evaluated by immunofluorescence (IF) analysis. Morphological changes were monitored under a bright field microscopy (Figure 14).

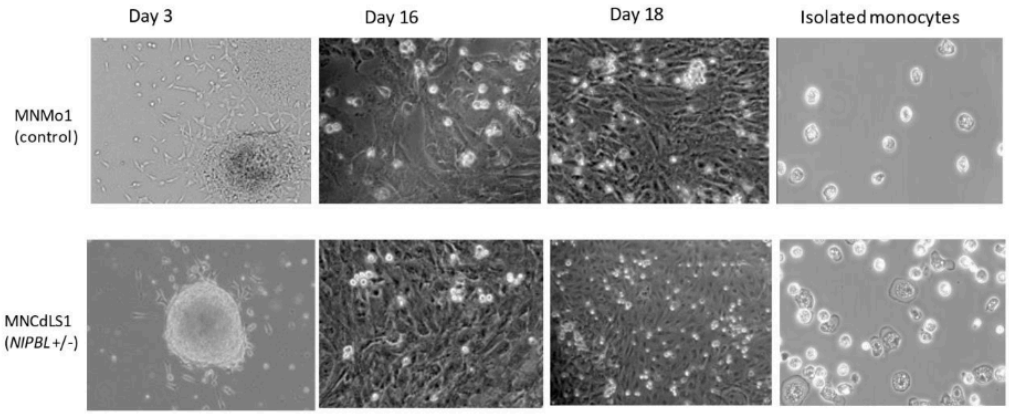

Figure 14. ***Morphology of cells at different stages of differentiation. Morphology of the cells were analyzed under microscopy in the bright field.***

The first difference between patient-derived cells and control cells was observed at day 3, when differentiation toward mesodermal cells was ongoing. In control cells, the presence of a central core and flattened cells indicated an active differentiation process, with small scattered cells surrounding them. In contrast, in the patient-derived cells, the differentiation process appeared delayed, and a stem cell-like morphology

was still observed at day 3. The morphology of monolayered HPCs appeared similar between patient-derived and control cells up to day 18. However, the number of floating MPCs recovered at day 14 was significantly lower in patient-derived cells, as shown in Figure 15.

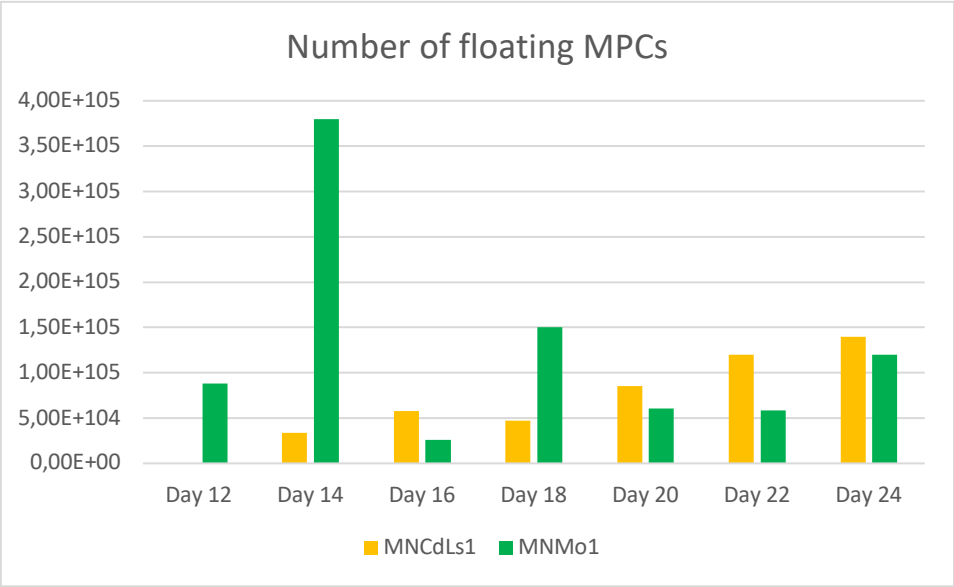

Figure 15. Time-course analysis of HPC production during differentiation. MNCdLS1 cells display delayed emergence (Day 14) and reduced progenitors output compared to control lines.

To define the characteristics of the differentiated cell populations, FACS analysis was performed using fluorescently conjugated antibodies against Tra-1-60 (iPSC stem cells), CD34 (hematopoietic stem cells), CD45 (hematopoietic cells), CD38 (lymphoid cells), CD14 (monocytes and macrophages), and CD11b (monocytes). Table I reports the percentage of gated cells expressing the different surface markers, while Figure 16 shows the percentage of monocytes defined as $CD34^{-}/CD45^{+}/CD14^{+}/CD11b^{+}$, regardless of CD38 expression. As shown in Table I, CD34-positive cells, representing hematopoietic stem/progenitor populations, decrease during differentiation, whereas CD45-positive cells increase, as expected. The monocyte population, characterized by double positivity for CD14 and CD11b, progressively increases during differentiation from HPCs to MPCs and finally to mature monocytes.

Stage of Differentiation	Cell Types	CD34+	CD45+	CD14+	CD11b+	CD38+
HPC	MNCdLS1	21,18	26,98	11,76	15,54	55,37
	MNMo1	26,11	27,15	7,79	11,56	51,92
	MNFa1	37,84	30,25	10,75	12,18	56,1
Myeloid Progenitor Cells	MNCdLS1	18,39	81,35	11,55	27,59	96,55
	MNMo1	32,26	83,88	21,67	37,05	88,47
	MNFa1	42,09	76,03	28,77	48,64	66,59
Monocytes	MNCdLS1	15,62	80,2	52,85	72,34	80,01
	MNMo1	12,19	81,48	67,11	72,42	84,48
	MNFa1	16,62	68,91	52,98	44,94	73,32

Table 1. ***Percentage of stage specific antibody expressing****. Cells at various stages of differentiation are harvested (20.000 cells/sample) and incubated with specific antibodies and utilized for FACS analysis.*

A. FACS on HPC (without consideration of CD38 positivity)

MNCdLS1

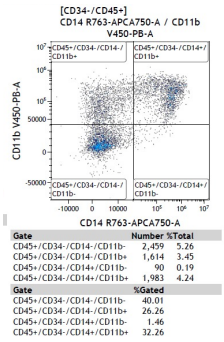

Gate	Number	%Total
CD45+/CD34-/CD14-/CD11b-	2,459	5.26
CD45+/CD34-/CD14-/CD11b+	1,614	3.45
CD45+/CD34-/CD14+/CD11b-	90	0.19
CD45+/CD34-/CD14+/CD11b+	1,983	4.24

Gate	%Gated
CD45+/CD34-/CD14-/CD11b-	40.01
CD45+/CD34-/CD14-/CD11b+	26.26
CD45+/CD34-/CD14+/CD11b-	1.46
CD45+/CD34-/CD14+/CD11b+	32.26

MNMo1

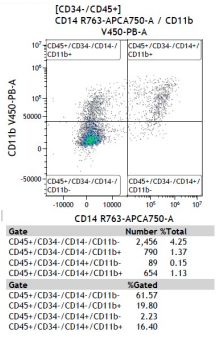

Gate	Number	%Total
CD45+/CD34-/CD14-/CD11b-	2,456	4.25
CD45+/CD34-/CD14-/CD11b+	790	1.37
CD45+/CD34-/CD14+/CD11b-	89	0.15
CD45+/CD34-/CD14+/CD11b+	654	1.13

Gate	%Gated
CD45+/CD34-/CD14-/CD11b-	61.57
CD45+/CD34-/CD14-/CD11b+	19.80
CD45+/CD34-/CD14+/CD11b-	2.23
CD45+/CD34-/CD14+/CD11b+	16.40

MNFa1

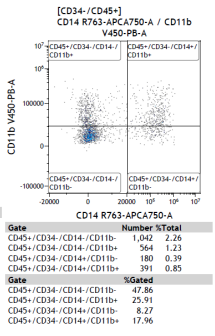

Gate	Number	%Total
CD45+/CD34-/CD14-/CD11b-	1,042	2.26
CD45+/CD34-/CD14-/CD11b+	564	1.23
CD45+/CD34-/CD14+/CD11b-	180	0.39
CD45+/CD34-/CD14+/CD11b+	391	0.85

Gate	%Gated
CD45+/CD34-/CD14-/CD11b-	47.86
CD45+/CD34-/CD14-/CD11b+	25.91
CD45+/CD34-/CD14+/CD11b-	8.27
CD45+/CD34-/CD14+/CD11b+	17.96

B. FACS on MPC (without consideration of CD38 positivity)

MNCdLS1

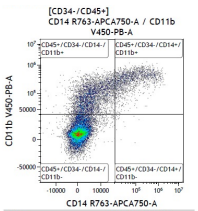

Gate	Number	%Total
CD45+/CD34-/CD14-/CD11b-	10,889	42.72
CD45+/CD34-/CD14-/CD11b+	3,830	15.03
CD45+/CD34-/CD14+/CD11b-	16	0.06
CD45+/CD34-/CD14+/CD11b+	1,701	6.67

Gate	%Gated
CD45+/CD34-/CD14-/CD11b-	66.25
CD45+/CD34-/CD14-/CD11b+	23.30
CD45+/CD34-/CD14+/CD11b-	0.10
CD45+/CD34-/CD14+/CD11b+	10.35

MNMo1

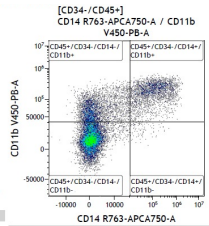

Gate	Number	%Total
CD45+/CD34-/CD14-/CD11b-	8,204	30.92
CD45+/CD34-/CD14-/CD11b+	3,129	11.79
CD45+/CD34-/CD14+/CD11b-	95	0.36
CD45+/CD34-/CD14+/CD11b+	2,517	9.49

Gate	%Gated
CD45+/CD34-/CD14-/CD11b-	58.83
CD45+/CD34-/CD14-/CD11b+	22.44
CD45+/CD34-/CD14+/CD11b-	0.68
CD45+/CD34-/CD14+/CD11b+	18.05

MNFa1

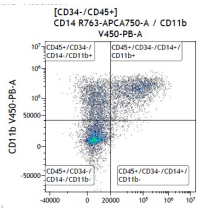

Gate	Number	%Total
CD45+/CD34-/CD14-/CD11b-	3,027	10.67
CD45+/CD34-/CD14-/CD11b+	2,340	8.25
CD45+/CD34-/CD14+/CD11b-	153	0.54
CD45+/CD34-/CD14+/CD11b+	2,493	8.79

Gate	%Gated
CD45+/CD34-/CD14-/CD11b-	37.78
CD45+/CD34-/CD14-/CD11b+	29.20
CD45+/CD34-/CD14+/CD11b-	1.91
CD45+/CD34-/CD14+/CD11b+	31.11

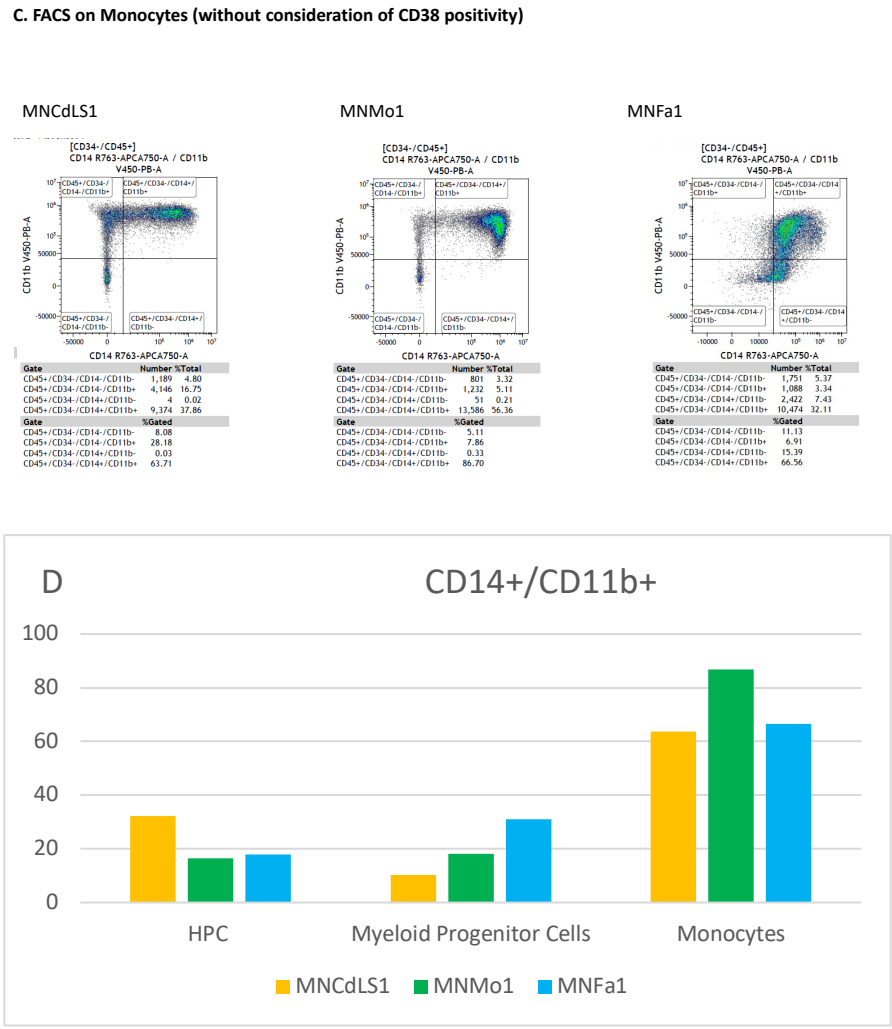

Figure 16. ***Percentage of CD11b+/CD14+ cells in the CD34-/CD45+ cell populations, without consideration of CD38 positivity.*** *Results obtained by FACS analysis performed on HPC (A), MPC (B) and Monocytes (C) are shown. Percentage of the CD14+/CD11b+ cells are shown in (D).*

When the percentage of the monocyte population is compared between the CdLS patient derived cells (MNCdLS1) and the respective control cells (MNMo1 and MNFa1), efficiency of monocyte production is inferior relative to MNMo1, as shown in Figure 16, when CD38 positivity is not considered. Initially, CD38 antibody was inserted as a negative control to exclude lymphocytic lineage. However, the situation is different. In fact, the monocytes produced in our *in vitro* system contained a good percentage of CD38 positive cells (more than 80%) in the control cells, while the CdLS patient derived differentiated monocytes are less positive in CD38 (40.3%) (Table II). When the positivity of CD14 and CD11b, separately calculated depending on the CD38 positivity, the production of

monocytes in the MNCdLS1 is inferior to the both of control cells in the CD38 negative monocytes, as shown in the Figure 17.

	CD38- (%)	CD38+ (%)
MNCdLS1	59,51	65,16
MNMo1	84,45	87,23
MNFa1	80,25	63,7

Table 2. ***CD38 positivity in monocyte population.*** *The percentage of the CD38 positive and negative cells are shown in the monocyte population*

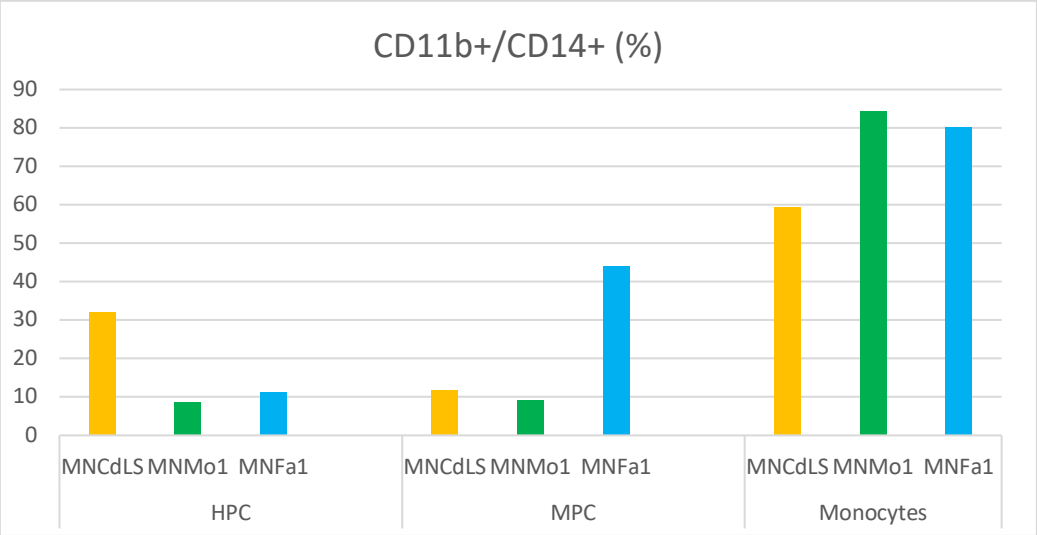

Figure 17. ***Percentage of CD34-/CD45+/CD38-/CD11b+/CD14+ cell population.*** *The percentage of CD11b+/CD14+ monocytes in the CD34-/CD45+/CD28- population is shown.*

Subsequently, the monocytes were differentiated in macrophages by the stimulation with M-CSF, and the produced macrophages were detected by Immuno fluorescent analysis using CD68 specific antibody (Figure 18). The monocytes derived from the CdLS patient are capable of differentiation into macrophages, which can be polarized into M1 and M2 type macrophages, as well as the respective control cells (data not shown).

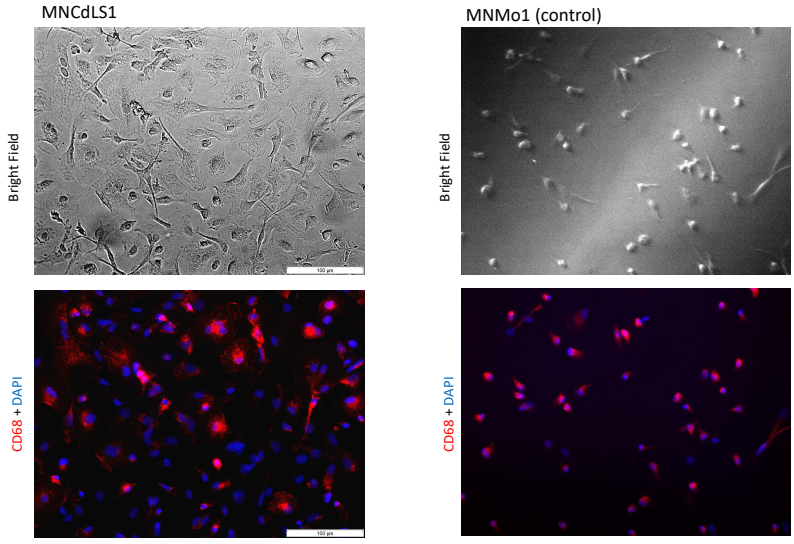

Figure 18. ***IF analysis of macrophages derived from monocytes in vitro****. The monocytes derived from the CdLS patient (MNCdLS1) and the control cells (MNMo1) were plated on glass circles precoated with poly-L-ornitine and Geltrex. Following incubation with M-CSF, monocytes were transformed into CD68 positive macrophages.*

On the bases of FACS and IF analysis, the CdLS patient derived iPSCs are proficient to be differentiated into myeloid cells as well as the respective control iPSCs. However, the efficiency of monocyte production is inferior to the control subjects. To define the difference in the quality of the CdLSpatient derived myeloid cells relative to the control cells, I have decided to perform transcriptomic analysis, presented in the next section.

4.4 Transciptomic analysis of CdLS patient derived myeloid cells

HPC, MPC and monocytes, derived from the CdLS patient (MNCdLS1) and the respective control cells (MNMo1), were harvested and RNA was extracted. The RNA seq analysis was performed in triplicate and the differentially expressed genes were searched for. Out of 27.465 genes analyzed, the number of differentially regulated genes (FDR<0.05) was indicated on the Table 3 in different types of comparisons. When the comparison between the samples derived from the patient (MNCdLS1) and those from her mother (MNMo1), although there are only hundreds of genes, the number of the differentially expressed genes increases along with differentiation stages, suggesting that the deficit of the hematopoiesis tends to occur at late stage of myeloid differentiation. Subsequently the pathway enrichment analysis was performed and the results are shown in Supplementary Figure S1. When the comparison is made between the

patient derived cells and the controls, significant down regulation was observed in monocytes in the gene sets responsible for α and γ interferon response, an inflammation and STAT 3 and STAT 5 signaling pathways in the monocyte populations. This suggests that the CdLS patient derived monocytes are defective in the homeostasis of immune responses. In fact, those pathways are most significantly up regulated during the differentiation from MPC to monocyte populations in both the CdLS patient derived cells and the controls.

Comparison	TOT	UP	DOWN
HPC_MNCdLS1vsMNMo1	121	86	35
MPC_MNCdLS1vsMNMo1	122	31	91
Monocytes_MNCdLS1vsMNMo1	530	407	123
MNCdLS_HPCvsMPC	8254	3192	5062
MNCdLS_MonocytesvsHPC	8563	3948	4615
MNCdLS_MonocytesvsMPC	2885	1957	928
MNMo1_HPCvsMPC	7443	3300	4143
MNMo1_MonocyesvsHPC	9411	4232	5179
MNMo1_MonocytesvsMPC	4597	2315	2282

Table 3. **The number of genes differentially regulated in different ways of comparison made on the RNAseq serustls** RNAseq analysis was performed on 27.465 genes and the number of differentially expressed gene (FDR<0.05) in various ways of comparison is indicated.

Subsequently, top 100 genes according to the fold change (2 >log 2fold change) were selected at different stages of differentiation out of all the differentially expressed genes (FDR<0.05). Top 100 genes are listed in the Supplementary Table S1; HPC, Table S2; MPC and Table 3S; Monocytes.

HPC		
	Category	Genes
UP	Chromatin	H3C3, H2BC3, CD84, STAG3, CBFA2T3, HPC
	Lymphoid lineage	LILRB4, TASL, TFYB2, IL16, BTK, FYB1, RASAL3, PRDM1, IRAG2, LCP2, PRKCB
	Ca+/K+ channels	P2RX1
	Cell adhesion and migration	SIGLEC14, BIN2, SELE, FERMT3
	Neural synapse	NRGN, DK10
	Zinc finger	PRDM1, ZNF597, ZNF468
DOWN	Chromatin	KDM5C
	Lymphoid lineage	PBX3
	inflammation	IFI44L, IFI44, IFI6, OAS2
	Cell cycle	CDKN2A
	Zinc finger	ZNF736, ZNF208, ZNF257
	WNT signaling	SOST

Table 4. ***Differentially expressed genes in CdLS patient derived HPC relative to the control cells, categorized according to biological functions****. Genes that are commonly regulated at least with either MPC or monocytes are indicated in red.*

MPC		
	Category	**Genes**
UP	Chromatin	H3C3
	Lymphoid lineage	BIVM
	Neural synapse	NCR3LG1
	Zinc finger	ZNF597, ZNF468
DOWN	Chromatin	KDM5C
	Lymphoid lineage	VEGFD, LCO102723996, CRLF1, NAV3, RORA, GCNT2, TIAM1
	Ion channels	SCN5A
	Cell adhesion and migration	EDN3, ADGRL3, FGF10, PECAM1, PCDHGA10, PTPRM, EPHB3
	Zinc finger	ZNF736, ZNF257, ZNP42, TSHZ2, ZNF248
	Tumor	TP63, ITH5, MTU52, NDN, MYCL, TIAM1, ARID38
	WNT signaling	WNT6, WNT28
	Ubiquitin	RNF144B, USP11, UBA1
	Inflammation	PRKCZ

Table 5. **Differentially expressed genes in CdLS patient derived MPC relative to the control cells, categorized according to biological functions** Genes that are commonly regulated at least with either HPC or monocytes are indicated in red.

Monocytes		
	Category	**Genes**
UP	Lymphoid lineage	LMCD1, CD200
	Cell adhesion and migration	LAMA4, FGG, FGF1, FGB
	Zinc finger	ZNF732
	Tumor	LOX, LZTS1
	WNT signaling	RSPO2, FRZB
	Inflammation	EREG
DOWN	Lymphoid lineage	LOC102723996, CD80, CD207, NCF1, GATA3, HLA-C
	Cell adhesion and migration	ADGRE1, ITGB7
	Zinc finger	ZNF736, ZNF257, ZNF208, ZNF562, ZNF410
	Tumor	TACSTD2, TNFAIPBL3, TNFRSF9, AXL
	Neural Development	NPTXR
	Inflammation	IL1A. IL7R, IFIT2, ADAM8, EBI3, MX2, IFNLR1, IRT1, USP18, RIG1, ISG20, STAT1, EIF2AK2
	Ubiquitin	TRIM6

Table 6. ***Differentially expressed genes in CdLS patient derived monocytes relative to the control cells, categorized according to biological functions*** *Genes that are commonly regulated at least with either HPC or MPC are indicated in red.*

The genes, whose expression is differentially regulated in the CdLS patient derived HPC, MPC and monocytes relative to the control cells, are listed in the Table 3 (HPC), Table 4 (MPC) and 5 (monocytes), respectively. They are categorized according to the biological functions. It is interesting to be noticed that some of the ZNF protein coding genes, such as ZNF736, ZNF257 and ZNF208, are commonly down regulated in HPC, MPC and monocyte populations. Strikingly, these ZNF genes are also down regulated in the patient derived iPSC as well as those upon differentiation into hepatocytes (Foglia *et al.*, 2024). In addition, ZNF 257 and ZNF 208 genes are located in the ZNF gene cluster on chromosome 19 p12-q13, where gene expression is significantly repressed due to the coverage of chromatins (Foglia M. et al.). In general, ZNF proteins are considered to work as repressors during embryogenesis. Hence, those ZNF gene down regulation could be the key genes responsible for the pathogenesis of CdLS and chromatinopathy.

It is also interesting to note that there are down regulated genes responsible for inflammation in the CdLS derived monocytes relative to the controls; ISG20 (Interferon stimulated exonuclease gene 20), STAT1 (Signal Transduction and Activation of transcription1) and EIF2AK2 (Enkaryotic Translation Initiation Factor 2 Alpha Kinase). All the genes are coding for proteins involved in the host defense response against viral and bacterial infections. This indicates that the monocytes differentiated from the CdLS iPSC shows deficits in the system of innate immunity. Lastly, the differentially expressed genes detected in all the differentiation stages (HPC, MPC and monocytes) code for proteins related to the lymphoid cell lineage, suggesting the presence of lymphoid cells due to leaky differentiation process during myeloid cell production.

Subsequently, I tried to understand gene networks involved in the differential expression of genes identified in the CdLS patient derived myeloid cell lineages. To obtain some information, Cytoscape analysis 51was performed, on the bases of the previous information. The results are shown in Figures 19-21. Cytoscape analysis is based on the search for gene sets or gene networks that are commonly regulated in the experimental group relative to the others.

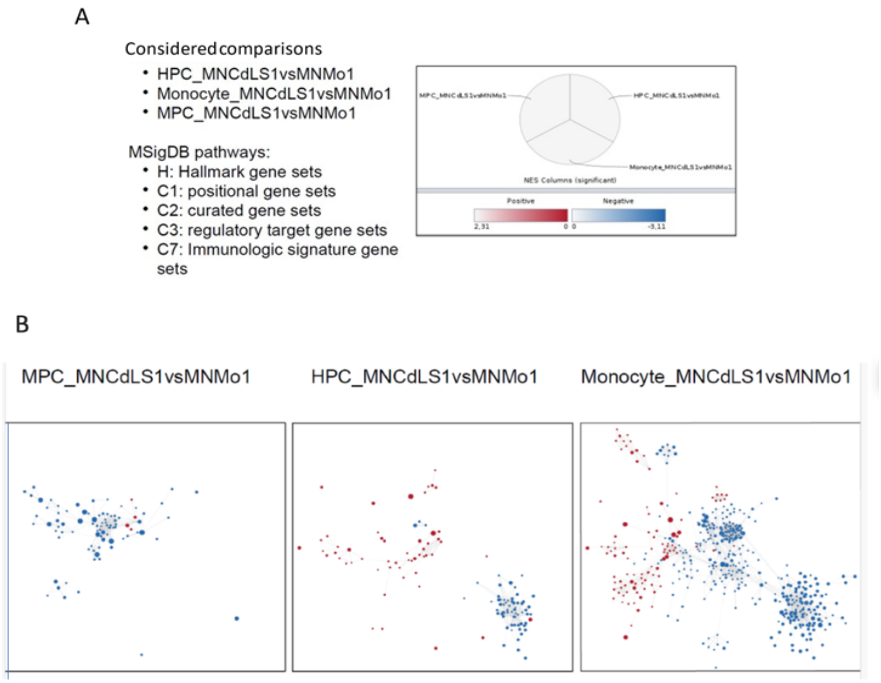

Figure 19. ***Differentially expressed gene sets between the CdLS patient derived cells and the control at different stages of differentiation.*** *Presentation of the Cytoscapes analysis is shown in A. In B, differentially expressed genes between the CdLS patient derived cells (MNCdLS1) and the control (MNMo1) at different stages of differentiation. Up regulated genes are shown in red, while down regulated genes are in blue.*

The differentially expressed gene sets of biological interests in the different stages of hematopoiesis (HPC, MPC and Monocytes) in the CdLS patient derived cells relative to the respective controls were selected and listed in the Figure 19A. As shown in Figure 19B, the number of differentially regulated gene sets connected as network increases along the process of differentiation. Some of the gene sets are clustered as sub-groups according to their functional similarity (Figures 20). Notably, up regulated gene sets in the CdLS patient derived monocytes relative to the healthy control cells are grouped in metabolism of glycoproteins, cell cycles and liver metabolisms. While the down regulated genes are clustered in 5 networks. In particular, the biggest gene cluster is the network related to lymphocyte functions, which suggests some dysregulation of differentiation along myeloid cell lineages.

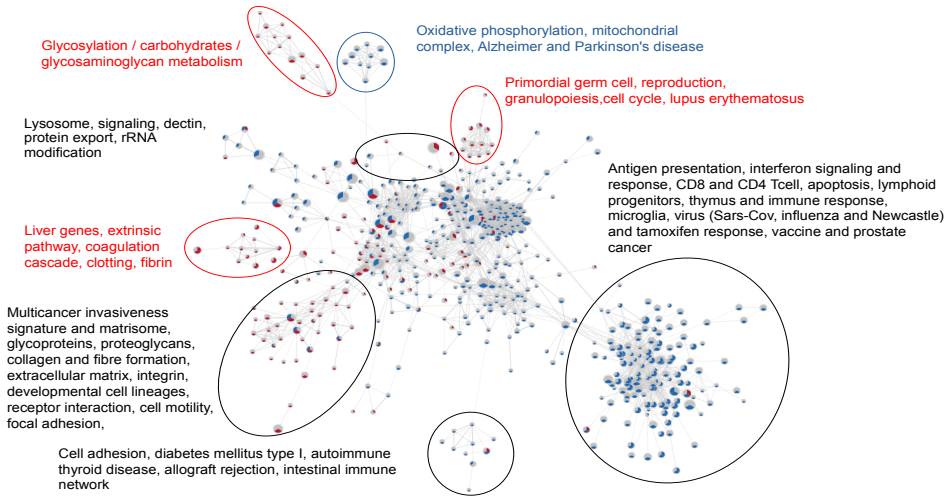

Figure 20. ***Network analysis focused on monocytes differentiation of the CdLS patient and respective controls****. Differentially up or down regulated gene sets in the CdLS patient derived monocytes compared to the healthy control monocytes are categorized (ah shown in figure 17B on the right panel) and grupoed according to their biological functions.*

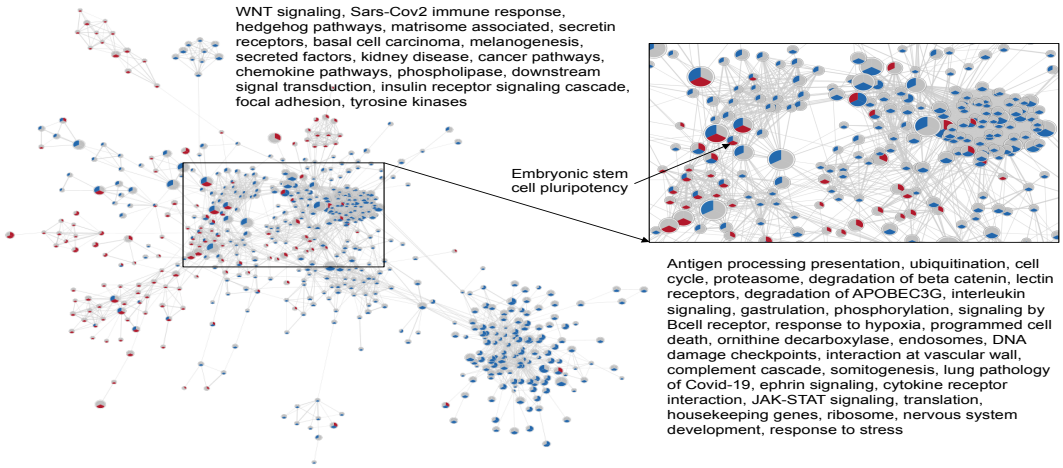

Figure 21. ***Network analysis focused on monocytes differentiation of the CdLS patient and the respective controls***

Another interesting observation is, as shown in Figure 21, the highly concentrated cluster of gene sets (which corresponds to the middle of the Figure 19) are related to antigen presentation and B cell function, suggesting the monocytes derived from the CdLS patient iPSC demonstrate some abnormal biological functions. In addition, the higher expression of genes responsible for the pluripotency in the CdLS patient derived monocytes relative to the healthy controls again suggest immature differentiation of the CdLS iPSC in the production of myeloid cell lineages.

CHAPTER 5 - DISCUSSION

In this thesis, I established the differentiation along myeloid hematopoiesis utilizing iPSC derived from a CdLS patient. As is expected, the patient derived iPSC is inferior to the respective healthy control cells in terms of efficiency of differentiation demonstrated by the analyses based on differentiation stage specific antibody recognition detected in FACS analysis. In addition, transcriptome analysis shows the enrichment of some biological pathways involved in inflammatory processes, cell adhesion, and cell migration during almost all stages of differentiation. In parallel, an upregulation of genes associated with the lymphoid lineage was also observed, suggesting a possible alteration of the transcriptional programs involved in the proper specification of the myeloid lineage.

Initially this study was aimed to understand the involvement of chromatinopathy in leukemogenesis. Because up to now, certainly in case of AML, probability to find coincidence of the disease with cohesinopathy. Thus, using the disease model, such as CdLS could be an alternative approach to understand the co-involvement of dysregulation of chromatin structure. In reality, it seems to be still difficult to observe such effects directly. What is detected in the analysis simply demonstrates that the efficiency of monocyte differentiation is lower, and seems to increase some lymphocytic lineage cells, suggesting dysregulated recognition of progenitor cells in every stage of differentiation.

During differentiation, it was observed that the number of macrophages obtained from patient-derived monocytes was lower than that of controls. This could indicate a reduced efficiency of the monocyte-to-macrophage differentiation process. However, further quantitative analyses will be needed to confirm this observation and assess its extent.
It will also be important to further investigate the characteristics of the obtained macrophages and their ability to polarize toward the M1 and M2 phenotypes. To this end, immunofluorescence analyses and quantitative assessments of specific markers associated with the two polarization states may be performed.
As described in the RNA-seq results section, patient-derived monocytes show alterations in the expression of genes involved in the innate immune response. These findings suggest a possible impairment of normal immune function and may also be linked to the activation of leukemogenesis-associated pathways observed during transcriptomic analysis. However, the direct role of chromatinopathy and NIPBL mutation in these alterations is not yet clear and will require further studies to be better understood.

Particularly in the FACS analysis, CD38 was used as a negative marker of differentiation along lymphoid cell lineages. However, in reality, a good percentage of CD38 positive cells were detected in the HPC, MPC and monocyte cell populations. It seems that the control cells derived from the healthy parents contain more CD38 positive cells than the patient derived cells. In fact, there are published works demonstrating that the CD38 positivity represents also the differentiation and transformation capacity of monocytes toward macrophages (Amici *et al.*, 2018). That suggests the CdLS patient derived monocytes could be less active in terms of biological availability of the monocytes.
Most interesting observation in the transcriptome analysis was the finding that some of the ZNF genes are commonly down regulated during differentiation from HPC, MPC and to monocytes. Those ZNF genes are also significantly down regulated in the CdLS patient derived iPSC as well as those following differentiation along hepatocytes (Foglia, sine data). Moreover, the previous results demonstrated that those genes form gene cluster where the gene expression is depressed because of abnormal chromatin localization. Human chromosomes encode more than 400 zinc finger proteins that potentially function as repressors of endogenous transposons during embryogenesis (Senft e Macfarlan, 2021). In particular, chromosome 19 contains several *ZNF* gene-clusters in the p12-13 and q13 genomic regions. The corresponding protein products are known as KRAB [Krueppel Associated Box Domain-containing Cys(2)-His(2) (C2H2 type)] zinc finger proteins (Lukic, Nicolas e Levine, 2014). These ZNF proteins are considered to be repressive transcription factors binding to the regulatory region of the *RNA polymerase II* gene. The p12-13 and q13 genomic regions are also bound to Heterochromatin Protein 1 (HP1: HP1α, β and γ) and SUV39H1/H2, a histone H3K9 methyl-transferase. These interactions may explain the repression of *RNA polymerase II* gene transcription (Vogel *et al.*, 2006). Finally, KAP1 [Krueppel-Associated Box (KRAB)-Associated Protein 1] is a transcription regulatory factor, which binds to the *KRAB-ZNF* loci and drives the epigenetic repression of many different genes during embryogenesis (Delfino, Shaffer e Smithgall, 2006; Rosspopoff e Trono, 2023). The *ZNF* gene cluster on chromosome 19p12, which contains the *ZNF208*, *ZNF257*, *ZNF676* and *ZNF728* genes, retains the DNA binding domains recognizing the *RNA polymerase II* promoter region and the typical coding sequence of the KRAB-ZNF proteins. Overall, the available information suggests that this cluster of *ZNF* genes, whose expression is repressed in *CdLS*-derived *iPSC*s and the differentiated cells derived from them, regulate master protein synthesis via histone modifications and DNA methylation.

To profound the transcriptome analysis at single cell level, where the certain population of the cells will be distinctively separated according to

the profile of transcripts. In this manner, we will have more possibility to understand the role of CD38 and other marker proteins. Now the project to perform the single cell RNA sequencing analysis is approved by Human Technopole facility. Thus, we are curious to obtain the results that could help us to identify the cell populations responsible for the CdLS deficits.

At last, I am interested in performing the hematopoiesis using other iPSC cells lines derived from CdLS patients carrying different type of mutations in cohesion complex. In fact, currently, we have obtained a new iPSC line derived from a CdLS patient carrying a missense mutation in SMCA1, a component of the Cohesin complex.

From the point of therapy in CdLS, as discussed in the Introduction, it is little trial that has been created. In fact, it is almost impossible to perform gene therapy, if the information of prenatal diagnosis is not performed properly during pregnancy. And gene therapy gives too much risk to fetuses. Thus, the treatment of the CdLS patients is limited to ones that potentially improve the pathological problems carried by the patients.

The analysis of iPSC derived differentiated cells is a possible way to identify genes and their protein products responsible for the pathogenesis of CdLS. In the previous study, the two gene loci were identified as the differentially expressed genes; DPP6 gene on chromosome 7q36.2 and the ZNF gene cluster on chromosome 19p12, as mentioned above. Currently, the forced expression of DPP6 gene in the CdLS patient derived iPSCs was obtained. We seek to see the improvement of differentiation capacity of those cells along hepatocyte lineage, cortical neurons and myeloid hematopoietic cells.

References

Ajmone, P.F. *et al.* (2014) «Communication, cognitive development and behavior in children with Cornelia de Lange Syndrome (CdLS): Preliminary results», *American Journal of Medical Genetics Part B: Neuropsychiatric Genetics*, 165(3), pp. 223–229. Available on: https://doi.org/10.1002/ajmg.b.32224.

Alonso-Gil, D. e Losada, A. (2023) «NIPBL and cohesin: new take on a classic tale», *Trends in Cell Biology*, 33(10), pp. 860–871. Available on: https://doi.org/10.1016/j.tcb.2023.03.006.

Amici, S.A. *et al.* (2018) «CD38 Is Robustly Induced in Human Macrophages and Monocytes in Inflammatory Conditions», *Frontiers in Immunology*, 9, p. 1593. Available on: https://doi.org/10.3389/fimmu.2018.01593.

Ascaso, Á. *et al.* (2024) «Espectro Cornelia de Lange», *Anales de Pediatría*, 100(5), pp. 352–362. Available on: https://doi.org/10.1016/j.anpedi.2024.03.002.

Avior, Y., Biancotti, J.C. e Benvenisty, N. (2015) «TeratoScore: Assessing the Differentiation Potential of Human Pluripotent Stem Cells by Quantitative Expression Analysis of Teratomas», *Stem Cell Reports*, 4(6), pp. 967–974. Available on: https://doi.org/10.1016/j.stemcr.2015.05.006.

Boyle, M. i. *et al.* (2015) «Cornelia de Lange syndrome», *Clinical Genetics*, 88(1), pp. 1–12. Available on: https://doi.org/10.1111/cge.12499.

Castiglioni, S. *et al.* (2022) «KMT2A: Umbrella Gene for Multiple Diseases», *Genes*, 13(3), p. 514. Available on: https://doi.org/10.3390/genes13030514.

Chatfield, K.C. *et al.* (2012) «Congenital heart disease in Cornelia de Lange syndrome: Phenotype and genotype analysis», *American Journal of Medical Genetics Part A*, 158A(10), pp. 2499–2505. Available on: https://doi.org/10.1002/ajmg.a.35582.

Chen, Z. *et al.* (2022) «Generation of an induced pluripotent stem cell line SJTUXHi001-A from an autism spectrum disorder patient carrying a heterozygous mutation in HDAC8 (p.P359S)», *Stem Cell Research*, 61, p. 102756. Available on: https://doi.org/10.1016/j.scr.2022.102756.

Closing the cohesin ring: Structure and function of its Smc3-kleisin interface (sine data). Available on: https://doi.org/10.1126/science.1256917.

Davidson, I.F. e Peters, J.-M. (2021) «Genome folding through loop extrusion by SMC complexes», *Nature Reviews Molecular Cell Biology*, 22(7), pp. 445–464. Available on: https://doi.org/10.1038/s41580-021-00349-7.

De Kouchkovsky, I. e Abdul-Hay, M. (2016) «'Acute myeloid leukemia: a comprehensive review and 2016 update'», *Blood Cancer Journal*, 6(7), pp. e441–e441. Available on: https://doi.org/10.1038/bcj.2016.50.

Deardorff, M.A. *et al.* (2012) «HDAC8 mutations in Cornelia de Lange Syndrome affect the cohesin acetylation cycle», *Nature*, 489(7415), pp. 313–317. Available on: https://doi.org/10.1038/nature11316.

Deardorff, M.A., Noon, S.E. e Krantz, I.D. (1993) «Cornelia de Lange Syndrome», in M.P. Adam et al. (a c. di) *GeneReviews®*. Seattle (WA): University of Washington, Seattle. Available on: http://www.ncbi.nlm.nih.gov/books/NBK1104/ (Consultato: 27 febbraio 2026).

Decroos, C. *et al.* (2014) «Compromised Structure and Function of HDAC8 Mutants Identified in Cornelia de Lange Syndrome Spectrum Disorders», *ACS Chemical Biology*, 9(9), pp. 2157–2164. Available on: https://doi.org/10.1021/cb5003762.

Delfino, F.J., Shaffer, J.M. e Smithgall, T.E. (2006) «The KRAB-associated co-repressor KAP-1 is a coiled-coil binding partner, substrate and activator of the c-Fes protein tyrosine kinase», *Biochemical Journal*, 399(Pt 1), pp. 141–150. Available on: https://doi.org/10.1042/BJ20060194.

Eckardt, J.-N. *et al.* (2023) «Alterations of cohesin complex genes in acute myeloid leukemia: differential co-mutations, clinical presentation and impact on outcome», *Blood Cancer Journal*, 13(1), p. 18. Available on: https://doi.org/10.1038/s41408-023-00790-1.

Emmerich, K. (sine data) «Protocol for differentiation of monocytes and macrophages from human induced pluripotent stem cells», *OPEN ACCESS* [Preprint].

Fazio, G. *et al.* (2017) «Impairment of Retinoic Acid Signaling in Cornelia de Lange Syndrome Fibroblasts», *Birth Defects Research*, 109(16), pp. 1268–1276. Available on: https://doi.org/10.1002/bdr2.1070.

Foglia, M. *et al.* (2024) «The NIPBL-gene mutation of a Cornelia de Lange Syndrome patient causes deficits in the hepatocyte differentiation of induced Pluripotent Stem Cells via altered chromatin-accessibility», *Cellular and Molecular Life Sciences: CMLS*, 81(1), p. 439. Available on: https://doi.org/10.1007/s00018-024-05481-z.

Foglia, M. (sine data) «The NIPBL-gene mutation of a Cornelia de Lange Syndrome patient causes deficits in the hepatocyte differentiation of induced Pluripotent Stem Cells via altered chromatin-accessibility».

Grados, M., Alvi, H. e Srivastava, S. (2017) «Behavioral and Psychiatric Manifestations in Cornelia de Lange Syndrome (CdLS)», *Current opinion in psychiatry*, 30(2), pp. 92–96. Avaiable on: https://doi.org/10.1097/YCO.0000000000000311.

Guerau-de-Arellano, M. (2018) «CD38 Is Robustly Induced in Human Macrophages and Monocytes in Inflammatory Conditions», *Frontiers in Immunology*, 9.

Heidinger-Pauli, J.M. *et al.* (2010) «Systematic Reduction of Cohesin Differentially Affects Chromosome Segregation, Condensation, and DNA Repair», *Current Biology*, 20(10), pp. 957–963. Avaiable on: https://doi.org/10.1016/j.cub.2010.04.018.

Huisman, S.A. *et al.* (2013) «High rate of mosaicism in individuals with Cornelia de Lange syndrome», *Journal of Medical Genetics*, 50(5), pp. 339–344. Avaiable on: https://doi.org/10.1136/jmedgenet-2012-101477.

Jahnke, P. *et al.* (2008) «The Cohesin loading factor NIPBL recruits histone deacetylases to mediate local chromatin modifications», *Nucleic Acids Research*, 36(20), pp. 6450–6458. Avaiable on: https://doi.org/10.1093/nar/gkn688.

Kawauchi, S. *et al.* (2009) «Multiple Organ System Defects and Transcriptional Dysregulation in the Nipbl+/− Mouse, a Model of Cornelia de Lange Syndrome», *PLoS Genetics*. A cura di W.A. Bickmore, 5(9), p. e1000650. Avaiable on: https://doi.org/10.1371/journal.pgen.1000650.

KAWAUCHI, S. *et al.* (2016) «Using Mouse and Zebrafish Models to Understand the Etiology of Developmental Defects in Cornelia de Lange Syndrome», *American journal of medical genetics. Part C, Seminars in medical genetics*, 172(2), pp. 138–145. Available on: https://doi.org/10.1002/ajmg.c.31484.

Kimbrel, E.A. e Lanza, R. (2016) «Pluripotent Stem Cells: The Last 10 Years», *Regenerative Medicine*, 11(8), pp. 831–847. Available on: https://doi.org/10.2217/rme-2016-0117.

Kline, A.D. *et al.* (2007) «Cornelia de Lange syndrome: Clinical review, diagnostic and scoring systems, and anticipatory guidance», *American Journal of Medical Genetics Part A*, 143A(12), pp. 1287–1296. Available on: https://doi.org/10.1002/ajmg.a.31757.

Kline, A.D. *et al.* (2018) «Diagnosis and management of Cornelia de Lange syndrome: first international consensus statement», *Nature Reviews Genetics*, 19(10), pp. 649–666. Available on: https://doi.org/10.1038/s41576-018-0031-0.

Kline, A.D., Barr, M. e Jackson, L.G. (1993) «Growth manifestations in the Brachmann-de Lange syndrome», *American Journal of Medical Genetics*, 47(7), pp. 1042–1049. Available on: https://doi.org/10.1002/ajmg.1320470722.

Laloraya, S., Guacci, V. e Koshland, D. (2000) «Chromosomal Addresses of the Cohesin Component Mcd1p», *The Journal of Cell Biology*, 151(5), pp. 1047–1056. Available on: https://doi.org/10.1083/jcb.151.5.1047.

Lee, G. *et al.* (2009) «Modeling Pathogenesis and Treatment of Familial Dysautonomia using Patient Specific iPSCs», *Nature*, 461(7262), pp. 402–406. Available on: https://doi.org/10.1038/nature08320.

Li, Z. *et al.* (2023) «Establishment of a transgene-free iPS cell line (SDQLCHi046-A) from a young patient bearing a HDAC8 mutation and suffering from Cornelia de Lange Syndrome», *Stem Cell Research*, 66, p. 102984. Available on: https://doi.org/10.1016/j.scr.2022.102984.

Liu, L. (2017) «Linking Telomere Regulation to Stem Cell Pluripotency», *Trends in Genetics*, 33(1), pp. 16–33. Available on: https://doi.org/10.1016/j.tig.2016.10.007.

Lukic, S., Nicolas, J.-C. e Levine, A.J. (2014) «The diversity of zinc-finger genes on human chromosome 19 provides an evolutionary mechanism for defense against inherited endogenous retroviruses», *Cell Death and Differentiation*, 21(3), pp. 381–387. Available on: https://doi.org/10.1038/cdd.2013.150.

Luzzani, S. *et al.* (2003) «Gastroesophageal reflux and Cornelia de Lange syndrome: Typical and atypical symptoms», *American Journal of Medical Genetics Part A*, 119A(3), pp. 283–287. Available on: https://doi.org/10.1002/ajmg.a.20191.

Malik, N. e Rao, M.S. (2013) «A Review of the Methods for Human iPSC Derivation», *Methods in molecular biology (Clifton, N.J.)*, 997, pp. 23–33. Available on: https://doi.org/10.1007/978-1-62703-348-0_3.

Mannini, L. *et al.* (2013) «Mutation Spectrum and Genotype–Phenotype Correlation in Cornelia de Lange Syndrome», *Human mutation*, 34(12), p. 10.1002/humu.22430. Available on: https://doi.org/10.1002/humu.22430.

Marchisio, P. *et al.* (2014) «Audiological findings, genotype and clinical severity score in Cornelia de Lange syndrome», *International Journal of Pediatric Otorhinolaryngology*, 78(7), pp. 1045–1048. Available on: https://doi.org/10.1016/j.ijporl.2014.03.038.

MartinsTaylor, K. e Xu, R. (sine data a) «Concise Review: Genomic Stability of Human Induced Pluripotent Stem Cells».

MartinsTaylor, K. e Xu, R. (sine data b) «Concise Review: Genomic Stability of Human Induced Pluripotent Stem Cells».

Mazzola, M. *et al.* (2019) «NIPBL: a new player in myeloid cell differentiation», *Haematologica*, 104(7), pp. 1332–1341. Available on: https://doi.org/10.3324/haematol.2018.200899.

Mazzola, M. *et al.* (2020) «Dysregulation of NIPBL leads to impaired RUNX1 expression and haematopoietic defects», *Journal of Cellular and Molecular Medicine*, 24(11), pp. 6272–6282. Available on: https://doi.org/10.1111/jcmm.15269.

Mikołajewska, E. (2013) «Interdisciplinary therapy in Cornelia de Lange syndrome - review of the literature», *Advances in Clinical and Experimental Medicine: Official Organ Wroclaw Medical University*, 22(4), pp. 571–577.

Mills, J.A. *et al.* (2018) «NIPBL+/− haploinsufficiency reveals a constellation of transcriptome disruptions in the pluripotent and cardiac states», *Scientific Reports*, 8(1), p. 1056. Available on: https://doi.org/10.1038/s41598-018-19173-9.

Moss, J. *et al.* (2017) «Genotype–phenotype correlations in Cornelia de Lange syndrome: Behavioral characteristics and changes with age», *American Journal of Medical Genetics Part A*, 173(6), pp. 1566–1574 Available on.: https://doi.org/10.1002/ajmg.a.38228.

Müller, F.-J. *et al.* (2011) «A bioinformatic assay for pluripotency in human cells», *Nature methods*, 8(4), pp. 315–317. Available on: https://doi.org/10.1038/nmeth.1580.

Nakamura-Ishizu, A., Takizawa, H. e Suda, T. (2014) «The analysis, roles and regulation of quiescence in hematopoietic stem cells», *Development*, 141(24), pp. 4656–4666. Available on: https://doi.org/10.1242/dev.106575.

Nasmyth, K. e Haering, C.H. (2009) «Cohesin: Its Roles and Mechanisms», *Annual Review of Genetics*, 43(1), pp. 525–558. Available on https://doi.org/10.1146/annurev-genet-102108-134233.

Okita, K. *et al.* (2008) «Generation of Mouse Induced Pluripotent Stem Cells Without Viral Vectors», *Science*, 322(5903), pp. 949–953. Available on: https://doi.org/10.1126/science.1164270.

Olley, G. *et al.* (2018) «BRD4 interacts with NIPBL and BRD4 is mutated in a Cornelia de Lange-like syndrome», *Nature genetics*, 50(3), pp. 329–332. Available on: https://doi.org/10.1038/s41588-018-0042-y.

Piché, J. *et al.* (2019) «The expanding phenotypes of cohesinopathies: one ring to rule them all!», *Cell Cycle*, 18(21), pp. 2828–2848. Available on: https://doi.org/10.1080/15384101.2019.1658476.

Rigotti, L. *et al.* (2025) «Cohesins: Crossroad Between Cornelia de Lange Spectrum and Cancer Predisposition», *American Journal of Medical Genetics Part A*, 197(8), p. e64076. Available on: https://doi.org/10.1002/ajmg.a.64076.

Rollins, R.A. *et al.* (2004) «Drosophila Nipped-B Protein Supports Sister Chromatid Cohesion and Opposes the Stromalin/Scc3 Cohesion Factor To Facilitate Long-Range Activation of the cut Gene», *Molecular and Cellular Biology*, 24(8), pp. 3100–3111. Available on: https://doi.org/10.1128/MCB.24.8.3100-3111.2004.

Rollins, R.A., Morcillo, P. e Dorsett, D. (1999) «Nipped-B, a Drosophila homologue of chromosomal adherins, participates in activation by remote enhancers in the cut and Ultrabithorax genes.», *Genetics*, 152(2), pp. 577–593. Available on: https://doi.org/10.1093/genetics/152.2.577.

Rosspopoff, O. e Trono, D. (2023) «Take a walk on the KRAB side», *Trends in genetics: TIG*, 39(11), pp. 844–857. Available on: https://doi.org/10.1016/j.tig.2023.08.003.

Selicorni, A. *et al.* (2021) «Cornelia de Lange Syndrome: From a Disease to a Broader Spectrum», *Genes*, 12(7), p. 1075. Available on: https://doi.org/10.3390/genes12071075.

Senft, A.D. e Macfarlan, T.S. (2021) «Transposable elements shape the evolution of mammalian development», *Nature Reviews Genetics*, 22(11), pp. 691–711. Available on: https://doi.org/10.1038/s41576-021-00385-1.

Sommer, C.A. *et al.* (sine data) «Induced Pluripotent Stem Cell Generation Using a Single Lentiviral Stem Cell Cassette».

Tsankov, A.M. *et al.* (2015) «An improved ScoreCard to assess the differentiation potential of human pluripotent stem cells», *Nature biotechnology*, 33(11), pp. 1182–1192. Available on: https://doi.org/10.1038/nbt.3387.

Umbach, A. *et al.* (2022) «Generation of corrected hiPSC clones from a Cornelia de Lange Syndrome (CdLS) patient through CRISPR-Cas-based technology», *Stem Cell Research & Therapy*, 13(1), p. 440. Available on: https://doi.org/10.1186/s13287-022-03135-0.

Vogel, M.J. *et al.* (2006) «Human heterochromatin proteins form large domains containing KRAB-ZNF genes», *Genome Research*, 16(12), pp. 1493–1504. Available on: https://doi.org/10.1101/gr.5391806.

White, G.E. e Erickson, H.P. (2009) «The Coiled Coils of Cohesin Are Conserved in Animals, but Not In Yeast», *PLoS ONE*. A cura di J. Langowski, 4(3), p. e4674. Available on: https://doi.org/10.1371/journal.pone.0004674.

Yusoff, Y.M. *et al.* (2019) «Identification of FLT3 and NPM1 Mutations in Patients with Acute Myeloid Leukaemia», *Asian Pacific Journal of Cancer Prevention : APJCP*, 20(6), pp. 1749–1755. Available on: https://doi.org/10.31557/APJCP.2019.20.6.1749.

Supplementary materials

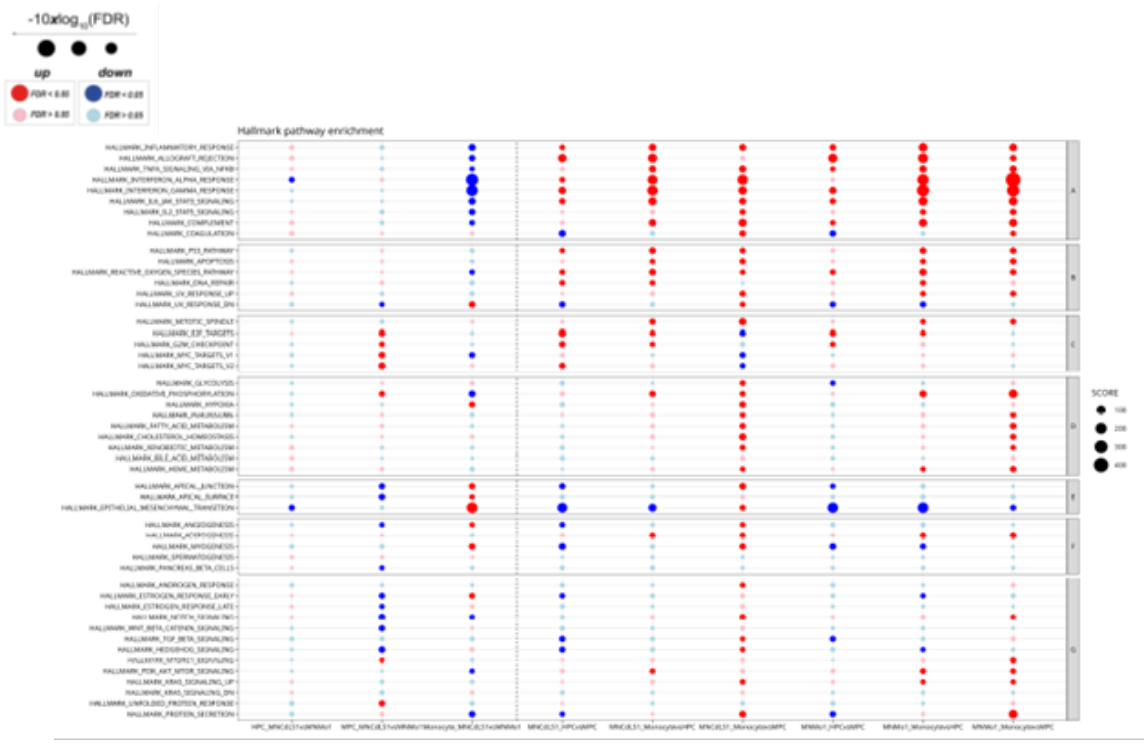

Supplementary Figure S1. ***Hallmark pathway enrichment analysis.*** Gene Set Enrichment Analysis (GSEA) was conducted as described in the method section. Signals used in the figure are indicated above.

Top 100 Upregulated Genes							
SYMBOL	ENTREZ	ENSEMBLE	CHROMOSOME	STAT	FOLD-CHANGE	P-VALUE	P-ADJ
LINC02864	400655	ENSG00000263711	18	7,525460347	9,360437319	5,25349E-14	2,32476E-10
FAM30A	9834	ENSG00000226777	14	5,403164518	8,557672579	6,54754E-08	5,43261E-05
CYP4F29P	54055	ENSG00000290541	21	6,220058205	8,503905106	4,9697E-10	7,33059E-07
LILRB4	11006	ENSG00000186818	19	4,477756715	6,662800163	7,54315E-06	0,002861117
SLC6A10P	386757	ENSG00000290985	16	3,757743485	6,058541189	0,000171453	0,032515968
ANKRD20A11P	391267	ENSG00000291280	21	5,165746484	5,933325463	2,39481E-07	0,000147871
LINC02327	102724917	ENSG00000258038	14	3,665048659	5,802114074	0,000247292	0,04129458
SLC30A8	169026	ENSG00000164756	8	5,599093061	5,404899653	2,15476E-08	1,9728E-05
VNN1	8876	ENSG00000112299	6	4,08077876	5,368951504	4,48851E-05	0,012037811
CYP4F3	4051	ENSG00000186529	19	5,338684901	5,171408164	9,36232E-08	7,5327E-05
HYAL4	23553	ENSG00000106302	7	5,845174921	5,076647894	5,06036E-09	5,59824E-06
FOLH1	2346	ENSG00000086205	11	5,197794783	4,270183238	2,01667E-07	0,000130596
KRT24	192666	ENSG00000167916	17	4,07042811	3,309505539	4,69268E-05	0,012336178
ABCC3	8714	ENSG00000108846	17	3,733041814	3,196247587	0,000189181	0,03512552
NXF3	56000	ENSG00000147206	X	4,498751444	3,099996474	6,83537E-06	0,002630231
DIO1	1733	ENSG00000211452	1	3,772612053	3,083193438	0,000161547	0,030857873
SIDT1	54847	ENSG00000072858	3	3,866275619	2,979758623	0,00011051	0,022745365
NME8	51314	ENSG00000086288	7	3,606847824	2,957485412	0,000309939	0,049730417
LINC02050	105377175	ENSG00000242781	3	4,169367806	2,562104065	3,05446E-05	0,009215783
GPR141	353345	ENSG00000187037	7	5,931999868	2,523525042	2,99267E-09	3,61174E-06
PPBP	5473	ENSG00000163736	4	3,849546507	2,517947526	0,000118337	0,024168909
H2BC3	3018	ENSG00000276410	6	4,169641427	2,501166643	3,05079E-05	0,009215783
MS4A10	341116	ENSG00000172689	11	3,776825808	2,497278632	0,00015884	0,030828483
TMEM207	131920	ENSG00000198398	3	4,126549131	2,48554869	3,68247E-05	0,010626738
LINC02461	105369740	ENSG00000258331	12	3,896401334	2,47340951	9,76326E-05	0,020624612
CYP4B1	1580	ENSG00000142973	1	4,737783531	2,461682524	2,16068E-06	0,001082421
LOC107985911	107985911	ENSG00000290846	2	6,084724073	2,401324671	1,16692E-09	1,63068E-06
LINC00923	91948	ENSG00000251209	15	3,90584154	2,330286923	9,3898E-05	0,020105537
LOC105376944	105376944	ENSG00000189229	3	7,71619546	2,278364281	1,19853E-14	6,36446E-11
RGS18	64407	ENSG00000150681	1	5,115726599	2,18746614	3,12535E-07	0,000188594
HSPA2	3306	ENSG00000126803	14	4,014786163	2,178225963	5,94997E-05	0,014903556
MAT1A	4143	ENSG00000151224	10	4,066472003	2,146608874	4,77302E-05	0,012424362
ZNF528	84436	ENSG00000167555	19	4,14414721	2,008732554	3,41081E-05	0,010175316
H3C3	8352	ENSG00000287080	6	6,413241337	1,982820074	1,42458E-10	2,27673E-07
CD84	8832	ENSG00000066294	1	4,089580328	1,923036898	4,32154E-05	0,011834164
KLB	152831	ENSG00000134962	4	4,572798724	1,915503504	4,81252E-06	0,002028211
TASL	80231	ENSG00000120280	X	4,113050629	1,874827744	3,90465E-05	0,011028966
SLC22A7	10864	ENSG00000137204	6	3,817538207	1,853147483	0,00013479	0,026908324
PLD4	122618	ENSG00000166428	14	3,626997652	1,849374276	0,000286736	0,046706288
FYB2	199920	ENSG00000187889	1	5,205232749	1,846941926	1,93754E-07	0,000130596
P2RX1	5023	ENSG00000108405	17	3,675863617	1,844667245	0,000237046	0,040344949
IL16	3603	ENSG00000172349	15	4,128805763	1,820324873	3,64652E-05	0,010626738
SNX20	124460	ENSG00000167208	16	3,968664756	1,81048182	7,22765E-05	0,01655593
SIGLEC14	100049587	ENSG00000254415	19	3,94795521	1,807970609	7,88215E-05	0,017379805
NRGN	4900	ENSG00000154146	11	4,109184292	1,805109661	3,97059E-05	0,011097176
BIN2	51411	ENSG00000110934	12	4,2495319	1,782510791	2,14218E-05	0,007010464
BTK	695	ENSG00000010671	X	5,327831037	1,737492058	9,93925E-08	7,76168E-05
TUBA4A	7277	ENSG00000127824	2	4,174112866	1,723015471	2,99149E-05	0,009215783
LINC00458	100507428	ENSG00000234787	13	3,609960726	1,72217165	0,000306243	0,049579681
LOC107986524	107986524	ENSG00000286339	6	4,695738807	1,721493718	2,65645E-06	0,001259488
PLG	5340	ENSG00000122194	6	4,400082821	1,71601802	1,0821E-05	0,003990378
LINC02882	100507377	ENSG00000251138	12	4,086246174	1,707107873	4,38409E-05	0,011877742
PTGS1	5742	ENSG00000095303	9	5,408733248	1,705640563	6,34721E-08	5,43261E-05

FYB1	2533	ENSG00000082074	5	4,96627093	1,65139866	6,82526E-07	0,000376076
PLEK	5341	ENSG00000115956	2	5,200076841	1,651115307	1,99206E-07	0,000130596
STAG3	10734	ENSG00000066923	7	3,695653295	1,586594271	0,000219322	0,038652586
ZNF790-AS1	284408	ENSG00000267254	19	3,86845222	1,560142228	0,000109528	0,02271944
AMN	81693	ENSG00000166126	14	3,672276979	1,555417954	0,000240399	0,040397669
RASAL3	64926	ENSG00000105122	19	3,895798277	1,552587294	9,78758E-05	0,020624612
CBFA2T3	863	ENSG00000129993	16	3,887531223	1,541327429	0,000101269	0,021171593
PRDM1	639	ENSG00000057657	6	6,675239151	1,524767566	2,46829E-11	5,95779E-08
SELE	6401	ENSG00000007908	1	3,777231849	1,521681234	0,000158581	0,030828483
ARHGAP15	55843	ENSG00000075884	2	3,683320532	1,505559057	0,000230215	0,039435152
COPS3P1	100652955	ENSG00000251643	4	3,97826314	1,499806718	6,94205E-05	0,016553637
LOC101927560	101927560	ENSG00000233008	1	4,089479117	1,486099197	4,32343E-05	0,011834164
ATP2A3	489	ENSG00000074370	17	4,603673543	1,431104113	4,15103E-06	0,001806787
APBB1IP	54518	ENSG00000077420	10	3,995483422	1,422844798	6,45624E-05	0,015872182
LINC00648	100506433	ENSG00000259129	14	5,833936934	1,421819641	5,41346E-09	5,74931E-06
MEP1A	4224	ENSG00000112818	6	3,672307015	1,416671996	0,000240371	0,040397669
IRAG2	4033	ENSG00000118308	12	3,748407714	1,410008834	0,000177961	0,033510901
LCP2	3937	ENSG00000043462	5	4,647668836	1,367352627	3,35707E-06	0,001536787
DGAT2	84649	ENSG00000062282	11	3,721205891	1,360697795	0,000198274	0,035652365
FERMT3	83706	ENSG00000149781	11	4,134279816	1,303646474	3,56069E-05	0,010504444
DGKB	1607	ENSG00000136267	7	4,290059804	1,272156146	1,78625E-05	0,006159315
ASRGL1	80150	ENSG00000162174	11	3,721968109	1,121418113	0,000197676	0,035652365
MYO1F	4542	ENSG00000142347	19	3,77319234	1,100873743	0,000161172	0,030857873
PRKCB	5579	ENSG00000166501	16	3,996703746	1,082537575	6,42306E-05	0,015872182
BCO2	83875	ENSG00000197580	11	3,720717662	1,065577841	0,000198657	0,035652365
DOCK10	55619	ENSG00000135905	2	3,698049065	1,059239536	0,000217263	0,038652586
ZNF597	146434	ENSG00000167981	16	3,975371248	0,961546732	7,02696E-05	0,016553637
ARHGAP45	23526	ENSG00000180448	19	3,721473601	0,895474035	0,000198064	0,035652365
ZNF468	90333	ENSG00000204604	19	4,253658882	0,879047488	2,10306E-05	0,00697978
GTF2H2C	728340	ENSG00000183474	5	4,21093971	0,815017437	2,54311E-05	0,008038335
PIK3CB	5291	ENSG00000051382	3	3,606027283	0,811954831	0,00031092	0,049730417
PTGR1	22949	ENSG00000106853	9	3,946794701	0,802198446	7,92044E-05	0,017379805
STX3	6809	ENSG00000166900	11	3,964242669	0,582919674	7,36293E-05	0,01655593

Top 100 Downregulated Genes							
SYMBOL	ENTREZ	ENSEMBLE	CHROMOSOME	STAT	FOLD-CHANGE	P-VALUE	P-ADJ
ZNF736	728927	ENSG00000234444	7	-8,81721946	-10,71605823	1,17337E-18	1,55771E-14
MEG3	55384	ENSG00000214548	14	-4,023762082	-10,36667902	5,72758E-05	0,014483136
ZNF208	7757	ENSG00000160321	19	-6,587640308	-9,870699282	4,46872E-11	9,88741E-08
LOC441666	441666	ENSG00000291065	10	-6,410361276	-9,174192511	1,45175E-10	2,27673E-07
LOC101930100	101930100	ENSG00000278932	21	-4,684811756	-6,156788912	2,80217E-06	0,001305272
ZNF257	113835	ENSG00000197134	19	-4,273091941	-5,953704655	1,92781E-05	0,006562213
SVIL-AS1	102724316	ENSG00000291093	10	-5,167757805	-5,475989708	2,36919E-07	0,000147871
LINC01629	105370578	ENSG00000258602	14	-5,081463178	-5,240406323	3,74539E-07	0,000216182
CASC11	100270680	ENSG00000249375	8	-5,075554784	-5,075117679	3,86367E-07	0,000218264
MIR381HG	378881	ENSG00000223403	14	-5,987603082	-4,929271123	2,12956E-09	2,69247E-06
SIGLEC12	89858	ENSG00000254521	19	-3,641396142	-3,272152574	0,000271164	0,044718401
IFI44L	10964	ENSG00000137959	1	-3,685596856	-3,243156675	0,000228167	0,039338114
IFI44	10561	ENSG00000137965	1	-3,826748456	-3,150472579	0,000129847	0,026317328
OAS2	4939	ENSG00000111335	12	-3,974755406	-3,098654599	7,04516E-05	0,016553637
RNVU1-28	124904616	ENSG00000277918	1	-4,598944782	-3,098434231	4,24636E-06	0,001818471
RPL21P28	100131205	ENSG00000220749	1	-6,409733632	-2,712000881	1,45774E-10	2,27673E-07
PKD1P2	283955	ENSG00000227827	16	-4,614265951	-2,313669613	3,94487E-06	0,001745671
IFI6	2537	ENSG00000126709	1	-4,039487021	-2,278219596	5,35682E-05	0,013675867
TTN-AS1	100506866	ENSG00000237298	2	-7,074783063	-2,190962309	1,49683E-12	4,96778E-09
LINC01410	103352539	ENSG00000238113	9	-3,741137472	-2,001561083	0,000183189	0,034252525
EIF2S3B	255308	ENSG00000180574	12	-4,505386618	-1,805326681	6,62522E-06	0,002586856
ZNF562	54811	ENSG00000171466	19	-5,874488768	-1,78154247	4,2415E-09	4,89635E-06
ERP27	121506	ENSG00000139055	12	-5,26088104	-1,75486918	1,43367E-07	0,000101278
NKX2-5	1482	ENSG00000183072	5	-4,124078473	-1,611188648	3,72222E-05	0,010626738
SOST	50964	ENSG00000167941	17	-3,720622099	-1,593111739	0,000198733	0,035652365
A1BG-AS1	503538	ENSG00000268895	19	-5,821608912	-1,585583774	5,82838E-09	5,9519E-06
XRRA1	143570	ENSG00000166435	11	-7,182759326	-1,271018093	6,83183E-13	2,59131E-09
CDKN2A	1029	ENSG00000147889	9	-3,662704781	-1,248375591	0,000249566	0,041413935
PPP1R14A	94274	ENSG00000167641	19	-3,634933391	-1,063530853	0,000278052	0,045571426
PLAGL1	5325	ENSG00000118495	6	-3,798578999	-1,023743805	0,000145528	0,028835188
DES	1674	ENSG00000175084	2	-3,977671243	-0,9992996	6,95935E-05	0,016553637
KDM5C	8242	ENSG00000126012	X	-5,520053436	-0,795486076	3,38897E-08	2,99935E-05
PBX3	5090	ENSG00000167081	9	-3,962391632	-0,735417541	7,42027E-05	0,01655593
USP9X	8239	ENSG00000124486	X	-3,963075316	-0,691168765	7,39904E-05	0,01655593
ANKRD50	57182	ENSG00000151458	4	-4,558680251	-0,616917464	5,14761E-06	0,002135533

Supplementary Table S1. Up and down regulated differentially expressed genes in MNCdLS1 relative to MNMo1 in HPC (100 genes).

Top 100 Upregulated Genes							
SYMBOL	ENTREZ	ENSEMBLE	CHROMOSOME	STAT	FOLD-CHANGE	P-VALUE	P-ADJ
LINC02864	400655	ENSG00000263711	18	6,854002238	8,540903799	7,1812E-12	1,40183E-08
FAM30A	5834	ENSG00000226777	14	5,210658662	7,575752521	1,88171E-07	0,000122443
CYP4F29P	54055	ENSG00000290541	21	5,024078293	6,914274355	5,05856E-07	0,000276089
ANKRD20A11P	391267	ENSG00000291280	21	5,315844876	6,894753553	1,06164E-07	8,44315E-05
HYAL4	23553	ENSG00000106302	7	4,887260145	6,482436452	1,02249E-06	0,000457415
LRRC37A11P	342666	ENSG00000290925	17	4,61242802	6,077621797	3,97992E-06	0,00144849
THBS2	7058	ENSG00000186340	6	4,138504104	5,604886396	3,49578E-05	0,008597876
LOC105376944	105376944	ENSG00000189229	3	11,8610265	5,392598881	1,88648E-32	4,05084E-28
DDX43	55510	ENSG00000080007	6	3,71584965	5,024065838	0,000202522	0,032453393
LCN9	392399	ENSG00000148386	9	4,284795422	4,429716829	1,82907E-05	0,005307528
PDE1C	5137	ENSG00000154678	7	3,826188573	3,803058653	0,000130143	0,023483633
LOC107986524	107986524	ENSG00000286339	6	8,104677237	3,121983168	5,28857E-16	2,27123E-12
LOC107985911	107985911	ENSG00000290846	2	5,113297332	2,919625625	3,16583E-07	0,000188833
CHCHD2	51142	ENSG00000106153	7	3,620436391	2,746669085	0,000294107	0,042102333
GPR176	11245	ENSG00000166073	15	3,768781868	2,570589808	0,000164046	0,028180507
COPS3P1	100652955	ENSG00000251643	4	5,875960193	2,471329453	4,20399E-09	5,31014E-06
YPEL3-DT	101928595	ENSG00000250616	16	5,5362317	2,380909468	3,09049E-08	3,1601E-05
LINC00926	283663	ENSG00000247982	15	4,20255006	2,030496793	2,63925E-05	0,006996615
TBC1D8B	54885	ENSG00000133138	X	3,877859494	1,780042816	0,00010538	0,020203705
H3C3	8352	ENSG00000287080	6	5,308546965	1,609098209	1,10503E-07	8,47437E-05
NCR3LG1	374383	ENSG00000188211	11	5,014250548	1,490905252	5,32406E-07	0,000276089
LOC389906	389906	ENSG00000285756	X	5,149082068	1,426937405	2,61764E-07	0,000160596
ZNF597	146434	ENSG00000167981	16	5,509917303	1,403822668	3,59002E-08	3,50403E-05
MRI1	84245	ENSG00000037757	19	4,455100582	1,133798697	8,38539E-06	0,002770145
CYBRD1	79901	ENSG00000071967	2	3,968888387	1,113653836	7,22087E-05	0,015201345
BIVM	54841	ENSG00000134897	13	4,796300981	1,044755766	1,61622E-06	0,000680494
ZNG1E	220869	ENSG00000147996	9	3,942704815	0,863065031	8,05678E-05	0,016321059
PPIE	10450	ENSG00000084072	1	5,017782954	0,846445784	5,22712E-07	0,000276089
ZNF468	90333	ENSG00000204604	19	3,636610633	0,784959581	0,000276249	0,041000078
DGKE	8526	ENSG00000153933	17	3,926475658	0,770675799	8,61996E-05	0,017138558
TRIM65	201292	ENSG00000141569	17	3,689013106	0,475860962	0,000225126	0,035285566

Top 100 Downregulated Genes							
SYMBOL	ENTREZ	ENSEMBLE	CHROMOSOME	STAT	FOLD-CHANGE	P-VALUE	P-ADJ
ZNF736	728927	ENSG00000234444	7	-9,263785457	-11,25571339	1,9731E-20	1,41228E-16
ATP2C2	9914	ENSG00000064270	16	-5,155681371	-7,57574526	2,5271E-07	0,000159601
EDN3	1908	ENSG00000124205	20	-3,713158907	-7,522631994	0,000204688	0,032557565
LOC441666	441666	ENSG00000291065	10	-5,226333104	-7,50329406	1,72905E-07	0,000116603
ALX4	60529	ENSG00000052850	11	-4,155527996	-7,28019347	3,24537E-05	0,008198573
PDZRN4	29951	ENSG00000165966	12	-4,116698175	-7,078478295	3,84339E-05	0,009169898
VEGFD	2277	ENSG00000165197	X	-3,971397668	-6,988523019	7,14522E-05	0,015191019
TP63	8626	ENSG00000073282	3	-4,170774925	-6,504533173	3,03566E-05	0,007853571
EYA2	2139	ENSG00000064655	20	-4,563558935	-6,483900921	5,02937E-06	0,001799927
WNT6	7475	ENSG00000115596	2	-4,482660229	-6,351649738	7,37183E-06	0,002553148
ITIH5	80760	ENSG00000123243	10	-3,72283354	-6,15723942	0,000196999	0,032148377
ZNF257	113835	ENSG00000197134	19	-4,30802292	-6,036827323	1,6472E-05	0,004981746
ZFP42	132625	ENSG00000179059	4	-4,372353984	-5,900306754	1,22914E-05	0,00382512
COL6A6	131873	ENSG00000206384	3	-4,288085921	-5,877046528	1,80219E-05	0,005301166
SYT7	9066	ENSG00000011347	11	-4,206847334	-5,847886802	2,58958E-05	0,006950755
SFN	2810	ENSG00000175793	1	-4,045672081	-5,831928112	5,21732E-05	0,011607171
LOC101930100	101930100	ENSG00000278932	21	-4,356772018	-5,746100713	1,31995E-05	0,004049029
CRLF1	9244	ENSG00000006016	19	-3,861633385	-5,715928773	0,000112631	0,021402974
LINC01629	105370578	ENSG00000258602	14	-3,831797198	-5,637342346	0,000127211	0,023346947
IQCA1	79781	ENSG00000132321	2	-3,630770606	-5,465530693	0,000282576	0,041001284
CYP24A1	1591	ENSG00000019186	20	-3,585819292	-5,119381069	0,000336022	0,047469682
MUC16	94025	ENSG00000181143	19	-3,804674069	-5,040435771	0,000141991	0,025198127
TSHZ2	128553	ENSG00000182463	20	-3,677445916	-4,974099573	0,000235581	0,036393028
MIR205HG	642587	ENSG00000230937	1	-4,094032337	-4,921003402	4,23935E-05	0,009994623
EYA4	2070	ENSG00000112319	6	-4,143358296	-4,899034855	3,42257E-05	0,008545669
LOC102723996	102723996	ENSG00000277117	21	-6,146177925	-4,550930758	7,93722E-10	1,2174E-06
TMTC1	83857	ENSG00000133687	12	-7,132025597	-4,13068187	9,89025E-13	\
ROR2	4920	ENSG00000169071	9	-4,260824791	-3,917552377	2,03674E-05	0,005724213
FAM184A	79632	ENSG00000111879	6	-4,084575862	-3,818330822	4,41574E-05	0,010195611
SLC35F3	148641	ENSG00000183780	1	-3,666562045	-3,689949221	0,000245833	0,037705559
PPL	5493	ENSG00000118898	16	-4,123872356	-3,555855081	3,72555E-05	0,008988632
CNR1	1268	ENSG00000118432	6	-5,462875095	-3,362875532	4,68484E-08	4,19157E-05
LINC02449	101927905	ENSG00000215241	12	-7,02211138	-3,327148959	2,1854E-12	4,69271E-09
ADGRL3	23284	ENSG00000150471	4	-4,246627433	-3,2631171	2,17012E-05	0,005974239
SCN5A	6331	ENSG00000183873	3	-4,382476154	-3,207752777	1,17338E-05	0,003705293
TEX14	56155	ENSG00000121101	17	-4,530499037	-3,164416026	5,88445E-06	0,002071424
NRXN1	9378	ENSG00000179915	2	-4,69870091	-3,039434195	2,61822E-06	0,001003945
DOCK9	23348	ENSG00000088387	13	-3,570160292	-3,039309746	0,000356763	0,049745251
DNAH8	1769	ENSG00000124721	6	-4,684192818	-2,961785408	2,81065E-06	0,001058827
COL17A1	1308	ENSG00000065618	10	-3,963678695	-2,922958427	7,38036E-05	0,015386253
FGF10	2255	ENSG00000070193	5	-3,655398354	-2,903401008	0,000256783	0,039105674
STEAP4	79689	ENSG00000127954	7	-4,468080963	-2,752891149	7,89244E-06	0,002648038
RNVU1-28	124904616	ENSG00000277918	1	-4,277617445	-2,614354885	1,88904E-05	0,005408456
MYH14	79784	ENSG00000105357	19	-3,829504209	-2,57264444	0,000128402	0,023365843
FOLR3	2352	ENSG00000110203	11	-3,833432812	-2,542940488	0,000126367	0,023346947
NAV3	89795	ENSG00000067798	12	-4,821799896	-2,438410142	1,42269E-06	0,000610987
FAM171B	165215	ENSG00000144369	2	-4,238133325	-2,430720502	2,25386E-05	0,006126217
CPAMD8	27151	ENSG00000160111	19	-3,756662554	-2,414496647	0,000172194	0,029345485
WNT2B	7482	ENSG00000134245	1	-4,417910844	-2,394982008	9,96595E-06	0,003242407
NPTXR	23467	ENSG00000221890	22	-4,000151856	-2,305337599	6,33019E-05	0,013592806
RNF144B	255488	ENSG00000137393	6	-4,723404131	-2,248193873	2,31929E-06	0,000922263
LINC00540	100506622	ENSG00000276476	13	-5,225413042	-2,228858229	1,73767E-07	0,000116603
RORA	6095	ENSG00000069667	15	-3,721702461	-2,223341385	0,000197884	0,032148377
PCDHGA10	56106	ENSG00000253846	5	-4,019740697	-2,137405446	5,82622E-05	0,012637019
KNDC1	85442	ENSG00000171798	10	-3,727620719	-2,130137565	0,000193296	0,031928035
ALOX15	246	ENSG00000161905	17	-5,239415381	-2,10011769	1,61086E-07	0,0001153
TBX3	6926	ENSG00000135111	12	-7,500019378	-2,091536055	6,38084E-14	2,2836E-10
MPZL2	10205	ENSG00000149573	11	-4,648935173	-2,0872386	3,33653E-06	0,001235264
SSTR2	6752	ENSG00000180616	17	-3,74534725	-2,069828425	0,000180144	0,030220635
AATK	9625	ENSG00000181409	17	-4,90614602	-2,035190209	9,28834E-07	0,000433584
RPL21P28	100131205	ENSG00000220749	1	-4,923256412	-2,007715437	8,51158E-07	0,000410994
PRKCZ	5590	ENSG00000067606	1	-3,910763049	-1,95078349	9,2005E-05	0,018124985
PTPRM	5797	ENSG00000173482	18	-5,011520968	-1,896588314	5,40015E-07	0,000276089
GCNT2	2651	ENSG00000111846	6	-3,735014511	-1,834479605	0,000187704	0,031244774
HK3	3101	ENSG00000160883	5	-4,920938387	-1,823860393	8,61302E-07	0,000410994
MTUS2	23281	ENSG00000132938	13	-4,029085581	-1,823832408	5,59942E-05	0,012269022
GAS8	2622	ENSG00000141013	16	-3,955858239	-1,810770454	7,62604E-05	0,015745568
PKD1P2	283955	ENSG00000227827	16	-3,652339282	-1,807593554	0,000259862	0,039140119
GFRA2	2675	ENSG00000168546	8	-4,136687435	-1,622355514	3,52356E-05	0,008597876
NDN	4692	ENSG00000182636	15	-3,622891383	-1,604879547	0,000291328	0,041984496
FHDC1	85462	ENSG00000137460	4	-4,058697117	-1,595021133	4,93473E-05	0,011154041
TTN-AS1	100506866	ENSG00000237298	2	-5,08332274	-1,549855305	3,70889E-07	0,000215246
MYRF	745	ENSG00000124920	11	-4,701830724	-1,517366167	2,57839E-06	0,001003945
CALHM2	51063	ENSG00000138172	10	-3,857015819	-1,501543546	0,00011478	0,021463228
MYCL	4610	ENSG00000116990	1	-4,773413678	-1,46455339	1,81129E-06	0,000747959
C3orf18	51161	ENSG00000088543	3	-3,678231871	-1,363506257	0,000234856	0,036393028
XRRA1	143570	ENSG00000166435	11	-7,214200343	-1,321425892	5,42518E-13	1,45619E-09
ITGA9	3680	ENSG00000144668	3	-3,856658308	-1,235231194	0,000114948	0,021463228
TIAM1	7074	ENSG00000156299	21	-4,471457114	-1,161556054	7,76884E-06	0,002647943
EPHB3	2049	ENSG00000182580	3	-4,091704201	-1,105206792	4,28215E-05	0,009994623
USP11	8237	ENSG00000102226	X	-3,947523059	-1,100729525	7,89639E-05	0,016148497
ZNF248	57209	ENSG00000198105	10	-3,636041415	-1,038439685	0,00027686	0,041000078
CDK16	5127	ENSG00000102225	X	-3,938775414	-0,941129386	8,18985E-05	0,016435584
PECAM1	5175	ENSG00000261371	17	-3,592613254	-0,882093338	0,000327378	0,046554928
STARD10	10809	ENSG00000214530	11	-3,777193538	-0,867184788	0,000158605	0,027465609
TPCN1	53373	ENSG00000186815	12	-3,5743873	-0,789043501	0,000351049	0,049268462
UBA1	7317	ENSG00000130985	X	-3,782151844	-0,784708714	0,000155478	0,027143001
KDM5C	8242	ENSG00000126012	X	-5,391072569	-0,777566397	7,00384E-08	5,78436E-05
SIPA1L1	26037	ENSG00000197555	14	-3,694815817	-0,756693377	0,000220046	0,034743036
ARPIN	348110	ENSG00000242498	15	-4,164984563	-0,714036809	3,11374E-05	0,007959674
ARID3B	10620	ENSG00000179361	15	-3,651557583	-0,64251828	0,000260655	0,039140119

Supplementary Table S2. Up and down regulated differentially expressed genes in MNCdLS1 relative to MNMo1 in MPC (100 genes).

Top 100 Upregulated Genes							
SYMBOL	ENTREZ	ENSEMBLE	CHROMOSOME	STAT	FOLD-CHANGE	P-VALUE	P-ADJ
BNC1	646	ENSG00000169594	15	6,128694994	8,901919189	8,86028E-10	7,92737E-07
TYRP1	7306	ENSG00000107165	9	4,253058329	8,627663704	2,10871E-05	0,002830016
LINC02864	400655	ENSG00000263711	18	6,869427126	8,558282405	6,44602E-12	1,25832E-08
FAM30A	5834	ENSG00000226777	14	5,298457061	8,395357629	1,16785E-07	4,73157E-05
ARSI	340075	ENSG00000183876	5	5,502753686	8,351546161	3,73905E-08	1,95826E-05
CDH3	1001	ENSG00000062038	16	5,040364516	8,08363679	4,64646E-07	0,000136732
NETO1	81832	ENSG00000166342	18	4,382327743	7,663427309	1,17418E-05	0,001895727
MAB21L2	10586	ENSG00000181541	4	4,41561093	7,528090751	1,00725E-05	0,001720135
NKAIN3	286183	ENSG00000185942	8	3,282869586	7,354338787	0,001027562	0,040411789
LAMA4	3910	ENSG00000112769	6	3,750632149	7,112826493	0,000176389	0,012337484
KRT8P3	728638	ENSG00000254285	8	4,312886553	7,078214909	1,61137E-05	0,002353803
CYP4F29P	54055	ENSG00000290541	21	5,103518792	7,016295612	3,33395E-07	0,00010847
KIAA1549L	25758	ENSG00000110427	11	3,383490065	6,787443102	0,000715708	0,032422779
KRT19	3880	ENSG00000171345	17	6,239772741	6,782208236	4,38207E-10	4,2771E-07
FGG	2266	ENSG00000171557	4	4,651724737	6,737842394	3,2917E-06	0,000679642
MASP1	5648	ENSG00000127241	3	4,503426211	6,733893421	6,68666E-06	0,001221144
HS6ST2	90161	ENSG00000171004	X	4,109094116	6,710786108	3,97214E-05	0,004389736
AFP	174	ENSG00000081051	4	3,921049231	6,601136851	8,81642E-05	0,007349377
SYNPO2	171024	ENSG00000172403	4	6,270765341	6,583729762	3,59278E-10	3,85739E-07
ACTG2	72	ENSG00000163017	2	4,555971408	6,54787368	5,2144E-06	0,000999722
NKAIN4	128414	ENSG00000101198	20	4,321105891	6,52297795	1,55249E-05	0,002299079
GREB1L	80000	ENSG00000141449	18	4,392040859	6,508395046	1,12292E-05	0,001857204
MAPK8IP1P1	644253	ENSG00000262500	17	3,472700452	6,498482858	0,00051525	0,025971749
RGS4	5999	ENSG00000117152	1	5,083909956	6,442462789	3,69743E-07	0,000114158
RSPO2	340419	ENSG00000147655	8	4,715667856	6,375185372	2,40919E-06	0,000522551
GABRA2	2555	ENSG00000151834	4	3,790676409	6,361052442	0,000150238	0,010862127
C2orf72	257407	ENSG00000204128	2	3,859854787	6,347815681	0,000113454	0,008989693
BDKRB1	623	ENSG00000100739	14	4,037869057	6,270943527	5,39389E-05	0,005387121
CPA4	51200	ENSG00000128510	7	4,170010188	6,268240138	3,04586E-05	0,003678785
CSDC2	27254	ENSG00000172346	22	4,326677594	6,256115456	1,51375E-05	0,002273064
FENDRR	400550	ENSG00000268388	16	3,501418567	6,232678419	0,000462788	0,024178722
LINC01162	104355138	ENSG00000232790	7	4,605374591	6,231708313	4,11724E-06	0,000818607
FGB	2244	ENSG00000171564	4	3,828792371	6,177342031	0,000128774	0,009736462
LMCD1	29995	ENSG00000071282	3	5,369730051	6,115413443	7,88546E-08	3,4556E-05
GDF6	392255	ENSG00000156466	8	5,48093609	6,065252328	4,23081E-08	2,16305E-05
LOX	4015	ENSG00000113083	5	5,673919344	6,017248589	1,39567E-08	8,09978E-06
CSPG4P13	100302666	ENSG00000260139	15	3,438109256	5,963565167	0,000585791	0,028347657
ANKRD20A11P	391267	ENSG00000291280	21	4,525383804	5,922784724	6,0286E-06	0,001115967
KCNK3	3777	ENSG00000171303	2	3,62306841	5,917621589	0,000291129	0,017735827
LCN9	392399	ENSG00000148386	9	4,803883985	5,872426235	1,55617E-06	0,000367205
SLC5A12	159963	ENSG00000148942	11	4,633291773	5,831745823	3,59897E-06	0,000729063
PLN	5350	ENSG00000198523	6	3,56051854	5,801609902	0,000370123	0,021108778
SH3RF2	153769	ENSG00000156463	5	6,530677863	5,770367918	6,54727E-11	9,37263E-08
ZNF732	654254	ENSG00000186777	4	4,107085026	5,752691116	4,00684E-05	0,004389736
LZTS1	11178	ENSG00000061337	8	4,386510231	5,73193496	1,15184E-05	0,001877477
FGA	2243	ENSG00000171560	4	4,191702161	5,616819155	2,76869E-05	0,00347278
ANXA8	653145	ENSG00000265190	10	5,415052553	5,606672793	6,12707E-08	2,79929E-05
FRZB	2487	ENSG00000162998	2	4,304027592	5,60326429	1,67721E-05	0,00240757
ST6GALNAC5	81849	ENSG00000117069	1	3,537614124	5,601327769	0,00040376	0,022511535
FREM2	341640	ENSG00000150893	13	4,048008072	5,563149075	5,16554E-05	0,005265044
CAV1	857	ENSG00000105974	7	4,299565212	5,546424181	1,71134E-05	0,00240757
HYAL4	23553	ENSG00000106302	7	4,184437811	5,546030628	2,85873E-05	0,003527899
FGF1	2246	ENSG00000113578	5	3,279772352	5,518411689	0,001038909	0,04063477
KCTD16	57528	ENSG00000183775	5	5,570056493	5,4799282	2,54657E-08	1,36706E-05
LUM	4060	ENSG00000139329	12	4,407856356	5,44517162	1,04399E-05	0,00175137
DSC3	1825	ENSG00000134762	18	5,208669079	5,413608794	1,902E-07	6,89772E-05
EREG	2069	ENSG00000124882	4	3,734323845	5,405995638	0,00018822	0,013037587
AQP4	361	ENSG00000171885	18	3,239062706	5,403840212	0,001199232	0,044706788
KRT8	3856	ENSG00000170421	12	5,082681621	5,361445471	3,72143E-07	0,000114158
CHST3	9469	ENSG00000122863	10	4,300144639	5,358488268	1,70687E-05	0,00240757
APOA1	335	ENSG00000118137	11	4,386076976	5,356631091	1,15413E-05	0,001877477
NSG1	27065	ENSG00000168824	4	4,043232191	5,33166021	5,27194E-05	0,005339825
RIMS1	22999	ENSG00000079841	6	3,224312221	5,302928119	0,001262756	0,046114232
ANXA8L1	728113	ENSG00000264230	10	3,869068582	5,290598405	0,000109252	0,008721064
VGLL3	389136	ENSG00000206538	3	4,274163467	5,29058233	1,91856E-05	0,002624031
DCN	1634	ENSG00000011465	12	4,299033144	5,285228177	1,71545E-05	0,00240757
ARSJ	79642	ENSG00000180801	4	3,773355208	5,244645907	0,000161067	0,011402668
NNMT	4837	ENSG00000166741	11	4,922840011	5,236709416	8,52972E-07	0,000215481
BGN	633	ENSG00000182492	X	3,595702579	5,223014588	0,000323517	0,019296906
AHSG	197	ENSG00000145192	3	3,596418095	5,219652652	0,000322629	0,019296906
HCN4	10021	ENSG00000138622	15	3,296206653	5,216712818	0,000979999	0,039369344
CLDN11	5010	ENSG00000013297	3	3,71060649	5,215462749	0,000206763	0,013910446
VAT1L	57687	ENSG00000171724	16	3,314881438	5,207016955	0,00091682	0,037734824
ZDHHC8BP	150244	ENSG00000290920	22	3,577700251	5,201965	0,000346631	0,020068958
C4BPB	725	ENSG00000123843	1	4,017734452	5,191128486	5,87604E-05	0,00566695
CNN1	1264	ENSG00000130176	19	4,145198104	5,182751857	3,3952E-05	0,003962236
CEMIP	57214	ENSG00000103888	15	5,85725433	5,132622273	4,70582E-09	3,48442E-06
ADAMTS9	56999	ENSG00000163638	3	4,375140742	5,129046244	1,21354E-05	0,001944655
COBL	23242	ENSG00000106078	7	3,215474918	5,12595617	0,001302289	0,047236565
KCTD8	386617	ENSG00000183783	4	3,552242973	5,121524288	0,000381962	0,021640817
LINC00842	643650	ENSG00000285294	10	3,234703527	5,101630791	0,001217691	0,044876326
MGAT4C	25834	ENSG00000182050	12	3,806631192	5,087519393	0,000140873	0,010395041
FGF5	2250	ENSG00000138675	4	3,265170962	5,087392134	0,00109398	0,041596695
LINC01638	105372978	ENSG00000233521	22	3,659775436	5,061466248	0,000252436	0,016084766
TRPC4	7223	ENSG00000133107	13	3,291534463	5,050491585	0,000996424	0,039603873
SGCE	8910	ENSG00000127990	7	3,306937724	5,033635255	0,000943219	0,038359342
PABPC4L	132430	ENSG00000254535	4	3,96405628	5,033625155	7,36869E-05	0,006592825
NR2F2	7026	ENSG00000185551	15	3,937062904	5,028630475	8,2485E-05	0,007048036
TBILA	112806053	ENSG00000261488	3	3,424467313	5,001483511	0,000616006	0,029459901
CDH3-AS1	123706523	ENSG00000260577	16	3,317265849	4,995429001	0,000909031	0,037659316
LRRN4	164312	ENSG00000125872	20	4,282923722	4,992047163	1,84453E-05	0,002538954
RASD1	51655	ENSG00000108551	17	4,500876331	4,991810021	6,76739E-06	0,001221144
CDH6	1004	ENSG00000113361	5	3,501593622	4,957174803	0,000462484	0,024178722
GCNT4	51301	ENSG00000176928	5	3,854105198	4,95104776	0,000116154	0,009169733
C6orf141	135398	ENSG00000197261	6	3,395104376	4,949318307	0,000686024	0,031476501
SPTBN2	6712	ENSG00000173898	11	5,698862992	4,94647119	1,20609E-08	7,194E-06
CMKLR2	2825	ENSG00000183671	2	3,560176664	4,913927966	0,000370605	0,021108778
GREM2	64388	ENSG00000180875	1	3,371981364	4,902211043	0,000746295	0,033109901
CD200	4345	ENSG00000091972	3	3,49269091	4,895873272	0,00047818	0,024688323
APCDD1L	164284	ENSG00000198768	20	3,523002384	4,886670509	0,000426688	0,023078743

Top 100 Downregulated Genes							
SYMBOL	ENTREZ	ENSEMBLE	CHROMOSOME	STAT	FOLD-CHANGE	P-VALUE	P-ADJ
ZNF736	728927	ENSG00000234444	7	-8,475916905	-10,303357	2,33235E-17	1,25206E-13
SLC35F1	222553	ENSG00000196376	6	-4,698461355	-6,506089586	2,62129E-06	0,000557296
ZNF257	113835	ENSG00000197134	19	-4,083438244	-5,741860742	4,43742E-05	0,004717068
LOC441666	441666	ENSG00000291065	10	-3,875610326	-5,635265064	0,000106358	0,008553635
LOC101930100	101930100	ENSG00000278932	21	-4,121915182	-5,461363499	3,75736E-05	0,004246405
ZNF208	7757	ENSG00000160321	19	-3,35330301	-5,13372713	0,000798532	0,034431496
LOC102723996	102723996	ENSG00000277117	21	-9,094641801	-4,862690244	9,48988E-20	2,03776E-15
TACSTD2	4070	ENSG00000184292	1	-3,674963654	-4,834747551	0,000237883	0,015371329
MMP12	4321	ENSG00000262406	11	-4,00183478	-4,798248967	6,28532E-05	0,005871418
KCNK12	56660	ENSG00000184261	2	-3,887758251	-4,776218316	0,000101174	0,008292046
TMTC1	83857	ENSG00000133687	12	-7,132420323	-4,421704749	9,86192E-13	2,64706E-09
CD207	50489	ENSG00000116031	2	-5,04028572	-4,351394663	4,64837E-07	0,000136732
L1TD1	54596	ENSG00000240563	1	-3,400227309	-4,27851083	0,000673299	0,031065426
SIGLEC12	89858	ENSG00000254521	19	-6,024648073	-4,242196597	1,69478E-09	1,34785E-06
MPZL2	10205	ENSG00000149573	11	-5,981467617	-4,115118906	2,21136E-09	1,69588E-06
OCA2	4948	ENSG00000104044	15	-3,340933129	-4,099100314	0,000834973	0,035433561
IL1A	3552	ENSG00000115008	2	-3,870853465	-3,91207967	0,000108455	0,008689753
LINC01169	102723165	ENSG00000259471	15	-3,463521696	-3,783773194	0,000533154	0,02643974
TNFAIP8L3	388121	ENSG00000183578	15	-4,094161942	-3,670983504	4,23698E-05	0,004549035
FAM171B	165215	ENSG00000144369	2	-6,39765303	-3,647186331	1,57783E-10	1,99299E-07
ATP1B2	482	ENSG00000129244	17	-5,461115528	-3,628575764	4,73152E-08	2,36279E-05
GATA3	2625	ENSG00000107485	10	-3,582088441	-3,573186961	0,000340858	0,01988927
DNAH8	1769	ENSG00000124721	6	-5,755520663	-3,278614343	8,63752E-09	6,18245E-06
PTGER3	5733	ENSG00000050628	1	-3,436710253	-3,228901457	0,000588825	0,028349422
PTENP1-AS	101243555	ENSG00000281128	9	-3,803674151	-3,09410884	0,000142566	0,010448167
IFNLR1	163702	ENSG00000185436	1	-3,96219728	-3,05981604	7,42631E-05	0,006616815
UBXN10	127733	ENSG00000162543	1	-3,302080606	-2,982752225	0,000959705	0,038809308
GAL	51083	ENSG00000069482	11	-3,37620918	-2,958183232	0,00073492	0,032876962
CLEC4F	165530	ENSG00000152672	2	-3,313985521	-2,901784751	0,000919763	0,037734824
ITGB7	3695	ENSG00000139626	12	-5,651646634	-2,830198913	1,58918E-08	8,98012E-06
IL7R	3575	ENSG00000168685	5	-3,426054369	-2,789924085	0,000612418	0,029353676
LINC00540	100506622	ENSG00000276476	13	-6,992851262	-2,781861815	2,69355E-12	6,10091E-09
DAB1	1600	ENSG00000173406	1	-3,249168639	-2,776283285	0,001157428	0,043450105
COLGALT2	23127	ENSG00000198756	1	-5,301955977	-2,743295701	1,14568E-07	4,73102E-05
GFRA2	2675	ENSG00000168546	8	-6,985363067	-2,725730177	2,8412E-12	6,10091E-09
OASL	8638	ENSG00000135114	12	-3,549550367	-2,70256263	0,00038589	0,021805811
C15orf48	84419	ENSG00000166920	15	-3,639173774	-2,697325868	0,000273514	0,016925563
CYP1B1	1545	ENSG00000138061	2	-3,650588403	-2,630656276	0,00026164	0,016430534
GLO1	2739	ENSG00000124767	6	-3,823349046	-2,618437084	0,000131651	0,009844134
LINC02449	101927905	ENSG00000215241	12	-6,155607306	-2,523465606	7,47903E-10	6,98249E-07
RPL21P28	100131205	ENSG00000220749	1	-5,714601161	-2,508364852	1,09962E-08	6,96474E-06
SECTM1	6398	ENSG00000141574	17	-3,709972877	-2,483041262	0,000207281	0,013910446
NPTXR	23467	ENSG00000221890	22	-4,290583985	-2,44799977	1,78204E-05	0,002468756
RSAD2	91543	ENSG00000134321	2	-4,197658693	-2,36938286	2,69689E-05	0,003447039
CD80	941	ENSG00000121594	3	-4,302148642	-2,368812905	1,6915E-05	0,00240757
ABCB4	5244	ENSG00000005471	7	-3,202238297	-2,352476794	0,001363641	0,048621632
IFIT1	3434	ENSG00000185745	10	-3,291925913	-2,320901584	0,000995038	0,039603873
NCF1	653361	ENSG00000158517	7	-3,935041305	-2,319744052	8,31824E-05	0,007059982
IFIT2	3433	ENSG00000119922	10	-3,414306709	-2,231801299	0,000639445	0,030136043
MAOA	4128	ENSG00000189221	X	-3,575731718	-2,22740846	0,00034925	0,02015978
EIF2S3B	255308	ENSG00000180574	12	-4,723952761	-2,158350005	2,31304E-06	0,000506816
STEAP4	79689	ENSG00000127954	7	-3,379393235	-2,122527998	0,00072646	0,032566345
GALM	130589	ENSG00000143891	2	-4,970884013	-2,110084414	6,66483E-07	0,000175835
TNFRSF9	3604	ENSG00000049249	1	-3,316900136	-2,067518765	0,000910221	0,037659316
USP18	11274	ENSG00000184979	22	-4,04764347	-2,01588741	5,17359E-05	0,005265044
ADAM8	101	ENSG00000151651	10	-4,22643019	-1,970355252	2,37428E-05	0,003135503
MX2	4600	ENSG00000183486	21	-3,504241415	-1,970229349	0,00045791	0,024178722
GPR35	2859	ENSG00000178623	2	-4,164176418	-1,924689105	3,12478E-05	0,003748519
TTN-AS1	100506866	ENSG00000237298	2	-6,058107551	-1,879680371	1,37732E-09	1,18301E-06
SP6	80320	ENSG00000189120	17	-3,594563199	-1,827763901	0,000324936	0,019327857
SERTM2	401613	ENSG00000260802	X	-3,373554725	-1,820799534	0,000742043	0,032989417
AKAP6	9472	ENSG00000151320	14	-3,953109301	-1,805658596	7,71422E-05	0,006733634
PPP1R16B	26051	ENSG00000101445	20	-3,346507805	-1,753979223	0,000818364	0,035005428
SIGLEC5	8778	ENSG00000268500	19	-3,696205608	-1,744115168	0,000218846	0,014370872
TTC39B	158219	ENSG00000155158	9	-4,566136979	-1,736858382	4,96794E-06	0,000966936
TRIM6	117854	ENSG00000121236	11	-3,76574643	-1,734489759	0,000166052	0,011690623
ADGRE1	2015	ENSG00000174837	19	-3,601242819	-1,699179842	0,0003167	0,01902638
B3GNT8	374907	ENSG00000177191	19	-3,680940045	-1,682058517	0,000232376	0,015120613
GSTM1	2944	ENSG00000134184	1	-4,190637551	-1,654700893	2,78172E-05	0,00347278
APBA1	320	ENSG00000107282	9	-3,306223561	-1,643534214	0,000945626	0,038384553
KCNC4	3749	ENSG00000116396	1	-3,717151888	-1,640470735	0,000201481	0,013691166
PLXNC1	10154	ENSG00000136040	12	-3,249675824	-1,573811691	0,001155366	0,043448653
RASGEF1A	221002	ENSG00000198915	10	-3,544320972	-1,54369921	0,000393626	0,022126506
TAS2R50	259296	ENSG00000212126	12	-3,351884766	-1,539328631	0,000802634	0,034539006
EBI3	10148	ENSG00000105246	19	-3,502662366	-1,530567369	0,000460633	0,024178722
RIGI	23586	ENSG00000107201	9	-6,258928936	-1,503653743	3,87631E-10	3,96361E-07
DNAJC15	29103	ENSG00000120675	13	-3,885941808	-1,459061799	0,000101934	0,008322537
PCDHGA10	56106	ENSG00000253846	5	-3,285388258	-1,456275079	0,001018419	0,040137081
MXD1	4084	ENSG00000059728	2	-3,527969081	-1,441080766	0,000418761	0,022880551
FHDC1	85462	ENSG00000137460	4	-3,694571143	-1,436521217	0,000220258	0,014419527
COLQ	8292	ENSG00000206561	3	-3,417739449	-1,428612984	0,000631435	0,029897648
ISG20	3669	ENSG00000172183	15	-4,018968212	-1,413697897	5,84536E-05	0,00566695
HELZ2	85441	ENSG00000130589	20	-3,202442452	-1,409946364	0,001362675	0,048621632
STAT1	6772	ENSG00000115415	2	-3,706213346	-1,388339056	0,000210381	0,013942942
ZNF562	54811	ENSG00000171466	19	-4,134419579	-1,242766446	3,55853E-05	0,004108187
MGLL	11343	ENSG00000074416	3	-4,116151791	-1,225677186	3,85251E-05	0,004331145
AXL	558	ENSG00000167601	19	-3,290172248	-1,217528725	0,001001261	0,039668028
FAM83G	644815	ENSG00000188522	17	-3,977785977	-1,216259173	6,95599E-05	0,006255756
EIF2AK2	5610	ENSG00000055332	2	-3,280222451	-1,186197769	0,001037253	0,04063477
CTSH	1512	ENSG00000103811	15	-3,786850887	-1,181865295	0,000152569	0,010924934
CCR5AS	102724297	ENSG00000223552	3	-4,041951658	-1,17091769	5,30082E-05	0,00534387
HLA-C	3107	ENSG00000204525	6	-3,485385184	-1,140901351	0,000491429	0,024961637
ERMP1	79956	ENSG00000099219	9	-3,845672566	-1,130145596	0,000120222	0,009319609
RIMS3	9783	ENSG00000117016	1	-3,7870944	-1,10424807	0,000152419	0,010924934
NQO2	4835	ENSG00000124588	6	-4,111148845	-1,070250697	3,93695E-05	0,004380217
PNPT1	87178	ENSG00000138035	2	-3,534343888	-1,015997118	0,000408789	0,022565354
SLC25A19	60386	ENSG00000125454	17	-3,404667577	-1,005159085	0,000662446	0,030780029
HNRNPLL	92906	ENSG00000143889	2	-4,001698162	-0,969725939	6,28895E-05	0,005871418
XRRA1	143570	ENSG00000166435	11	-5,223980172	-0,943460458	1,75118E-07	6,59702E-05
ZNF410	57862	ENSG00000119725	14	-3,197798824	-0,928347884	0,001384809	0,049069296

Supplementary Table S3. Up and down regulated differentially expressed genes in MNCdLS1 relative to MNMo1 in Monocytes (100 genes).